DEFLECTION MINIMIZATION OF PRESTRESSED CONCRETE GIRDERS

A Thesis

by

HEMANGI BIPIN AGARWAL

Submitted to the Office of Graduate and Professional Studies of
Texas A&M University
in partial fulfillment of the requirements for the degree of

MASTER OF SCIENCE

Chair of Committee,	John B. Mander
Committee Members,	Mary Beth D. Hueste
	John M. Nichols
Head of Department,	Robin Autenrieth

May 2020

Major Subject: Civil Engineering

ABSTRACT

When constructing prestressed concrete girder bridge structures, the high initial pretensioned force at the bottom of the girder causes it to camber upwards. This hogging of girders may be reduced slightly after casting the deck slab, any residual camber becomes locked-in. The upward deflection is generally mitigated by providing haunches or variable slab thickness. Such adjustments lead to construction delays, increased costs, and if not properly dealt with, rider discomfort. Because of loss of prestress over time, increase in strength of concrete after release and variations in production factors, the accurate estimation of long-term deflections may be complicated. Therefore, accurate predictions and minimization of camber and deflections should be, ideally incorporated into the design process.

The aim of this research is to achieve the deck profile as flat as possible under the dead load (after long-term losses). The magnitude of camber is analyzed, and methods devised to minimize the after-losses deflections by manipulating the prestress in terms of profile and magnitude of force. The proposed relations between optimum force and eccentricity for different harping points, provide significant improvements to the long-term deflections of precast prestressed concrete beams compared to the currently observed deflections for eccentric and harped tendon profiles.

ACKNOWLEDGEMENTS

I would like to thank my committee chair, Dr. John B. Mander for giving me the opportunity to do research and providing invaluable guidance throughout this research. He has taught me the methodology to carry out the study and to present the research works as clearly as possible.

I am thankful to my committee members, Dr. Mary Beth Hueste from Zachry Department of Civil and Environmental Engineering and Dr. John Nichols from the Department of Construction Science, for their guidance and support throughout the course of this research.

Thanks to my colleagues, my friends and the department faculty and staff for making my time at Texas A&M University a great experience.

Finally, I am extremely grateful to my parents for their encouragement and patience.

CONTRIBUTORS AND FUNDING SOURCES

Contributors

This work was supported by a thesis committee consisting of Professor John Mander (advisor) and Professor Mary Beth Hueste of the Department of Civil and Environmental Engineering and Professor John Nichols of the Department of Construction Science.

All other work conducted for the thesis (or) dissertation was completed by the student independently.

Funding Sources

There are no outside funding contributions to acknowledge related to the research and compilation of this document.

TABLE OF CONTENTS

Page

LIST OF FIGURES

Page

LIST OF TABLES

Page

1. INTRODUCTION

1.1. Background

Prestressing is a process to increase the flexural resistance of concrete and to control deflections by introducing permanent stresses in the member. The stresses created tend to counteract the stresses due to external loadings (Naaman, 2004). Along with counteracting the stresses, prestressing also helps to counteract the deflections due to gravity loading (self-weight and external loading) as shown in Figure 1-1. This helps in achieving larger span to depth ratios without compromising the serviceability of the structure. Prestressing strands provide eccentric axial compression force, making the prestressed concrete member camber up.

In order to minimize force and maximize eccentricity, high-strength steel strands are placed towards the bottom of the girder. While for a simply supported beam, load balancing of self-weight with draped post-tensioning strands can theoretically balance deflections as well, such task is not perfectly doable, with only eccentric prestressing strands. Harped pre-tensioning may partially balance dead loads and deflections, but generally in this case, the girders end up with an upward camber. The hogging deflection is reduced somewhat after the deck is cast, but any deflections are ‘locked-in’ once the concrete hardens. Some limited sagging will take place as the prestress losses, creep, and shrinkage effects continue to develop over time, but it is likely that a net upward deflection will still remain. Because the stiffness of the composite structure is much higher than that of the girder, the camber beyond the time of deck placement is considerably stabilized.

The individual segments of the bridge end up looking like hogged up segments. While these hogged up segments may be structurally adequate, they may not be as accepted for serviceability by the riders. Generally, these deflections are dealt with during the construction by providing variable depth haunches to form the deck slab. Sometimes, even these usual mitigation practices cannot make the girder fit into the bridge elevation profile and have to be casted again (Rizkalla et al., 2011). Therefore, it is necessary to shift the idea of using pre-tensioning strands, from only a strength point-of-view to a new concept: deflection balancing. Simply by changing the number and layout of pretensioned strands, the long-term deflection of the girders can be reduced.

The combined effect of shrinkage and creep of concrete along with the relaxation of prestressing steel causes the deflection to increase with time under sustained loading (Figure 1-2). In addition to the time-dependent properties of the materials, camber of the prestressed concrete member is affected by on-site parameters such as storage conditions, age of loading, etc. which cannot be accurately predicted during the design and planning stage of a project. The variation in these parameters could likely lead to errors in the estimation of camber. Although many researchers have been working on the accurate prediction of losses and camber/deflection for more than half a century, various agencies still experience an increasing instance of problems resulting from the deviation of the field camber from the theoretical prediction. If the camber is overestimated, additional asphalt or deck concrete would be required to achieve good ride quality. This leads to an increase in cost of construction and also increases the dead weight on the structure without increasing its strength. Additionally, if adjacent girders have a difference in erection

camber, it can lead to alignment problems during construction which are very difficult to overcome.

This research focuses on estimating and minimizing the long-term camber and deflections of pretensioned concrete members to achieve a nearly flat deck profile under dead load (after long-term losses). Prototype bridge designs shall be presented for eccentric and harped tendon profile for each un-topped and topped cases and the results of prestressing are compared with one another.

1.2. Research Objectives

The key objective of this research is to minimize the overall long-term deflection due to dead load and achieve a nearly flat deck profile. The objective second in order is to minimize the force after losses, while also minimizing the long-term deflections. To accomplish these objectives, the following tasks will be completed:

- Review literature on the existing models available for prediction of long-term camber and deflection of prestressed concrete members
- Develop relations between force and eccentricity for different harping points for an untopped (non-composite) case to obtain minimum long-term deflection using eccentric and harped tendon profiles
- Develop bridge design examples for the untopped case incorporating the optimum relations between force and eccentricity
- Extend deflection balancing concept to a topped (composite) case to minimize deflections using eccentric and harped tendon profiles

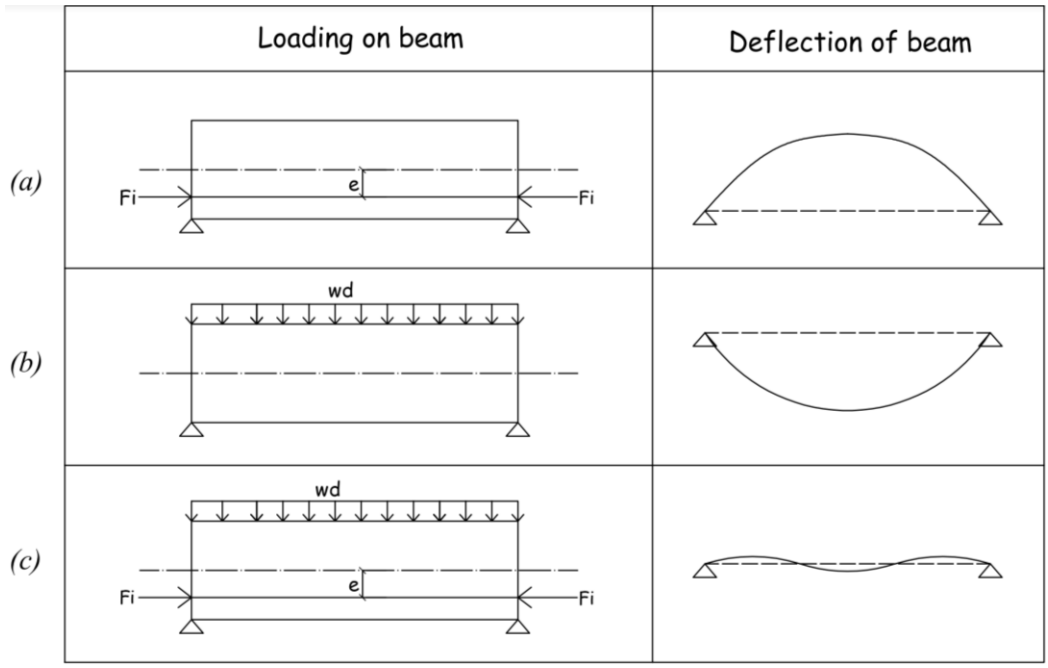

Figure 1-1: (a) Deflection due to prestressing force (b) deflection due to dead load, (c) net deflection due to prestressing force and dead load

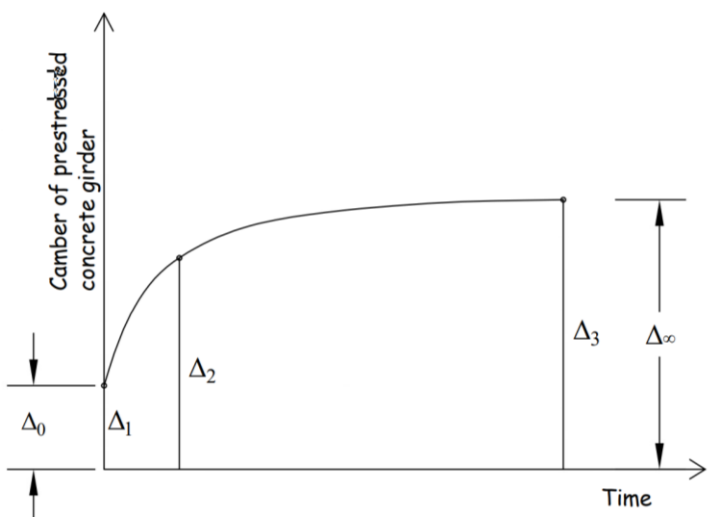

Figure 1-2: Change in camber of a precast prestressed concrete beam with time

- Develop bridge design examples for the topped case considering various ages of girder erection and comparing their effects on the long-term deflections

1.3. Organization of the Thesis

Chapter 2 of the thesis discusses the review of the relevant existing work and literature on accurate prediction methods for camber and factors affecting the long-term camber and deflection of prestressed concrete members. The parameters associated with various existing models for the prediction of camber are compared.

Chapter 3 uses the concept of deflection balancing for the untopped bridge girder for an eccentric and harped tendon profile. This includes developing harping distance versus deflection, force and end eccentricity charts. Bridge design examples using five numbers of modified Tx62 girders with 51 mm of asphalt on top for bridge of span 30.5 m are developed. The pretensioning designs are based on minimal force design and optimized prestress design which minimizes long-term deflections when eccentric-only and harped tendon profiles are used. The long-term deflections for both design approaches are compared.

Chapter 4 expands the concept of deflection balancing to the topped bridge girders having a cast-in-place concrete deck on the top. Different design examples are developed considering variable ages at which the girders are being erected and corresponding creep coefficients and loss percentages for each example. The most probable case of girder erection is considered and minimized; five numbers of Tx62 girders with a topping of 216 mm cast-in-place concrete is considered to develop an example of bridge of span 30.5 m.

Chapter 5 presents the general findings and conclusions drawn from the research based on the results and comparison of optimized prestress designs to minimize deflections vs deflections resulting from using minimal force design.

1.4. Research Questions Arising

From the current practices and the observed long-term camber in field, the following research questions arise:

1. If the prestress is to remain straight and eccentric, how can the force and eccentricity be optimized for both topped and untopped cases, to obtain the desirable flat-as-possible outcome after losses?
2. If a harped solution is possible, what should be the harping distance and central and end eccentricities for the girder cross-section for both topped and untopped cases and how can this be made up (in practical terms) in terms of the number of straight v/s harped tendons?
3. For the topped case, what is the effect of variation in the age of erection of girder considering eccentric and harped tendon profiles on the long-term deformation of the bridge?

2. LITERATURE REVIEW

2.1. Introduction

In the past, many studies have illustrated the consequences of overestimated or underestimated deflections in prestressed concrete members (Rosa et al. (2007), Tadros et al. (2011), Rizkalla et al. (2011), O'Neill and French (2012), Honarvar et al. (2015)). The combination of prestressing force along with the self-weight of the girder causes a net upward deflection at the midspan of the girder. This upward deflection helps to balance the downward deflection due to the superimposed dead loads and live loads, thus reducing the final sag of the girder over time. Camber is influenced by a number of interdependent variables, which may change with the passage of time. The accurate prediction of camber is thus complex yet significant for the construction and serviceability of prestressed concrete bridges. The four most significant variables found to affect long-term deflection and camber the concrete material properties, concrete creep and shrinkage and the initial prestressing force applied. A brief review of literature based on previous research on the influence of these factors on camber and the overall prediction of camber is presented in this chapter. There are many models like *fib* Model Code 2010, GL-2000, ACI 209R-92, AASHTO LRFD (2017), B3 available for estimating these parameters.

2.2. Factors affecting Long-term deflection

The camber of prestressed concrete beams is significantly dependent on the material properties of concrete. This section presents an introduction on properties of concrete like f'_c and E_c, and the creep, shrinkage, the losses in prestressing force. Other important

factors like effect of temperature along the depth of the beam, curing method and duration, storage conditions are also discussed.

2.2.1. Concrete strength

The compressive strength at 28-days is often used as a constant for the compressive strength of concrete at any age, but concrete strength actually varies over time and is widely affected by variables like aggregate size and curing history. Since the concrete strength is changing quickly during the release of prestress, prediction of concrete strength with time should be taken into account.

Since the modulus of elasticity is directly proportional to the compressive strength, the increased compressive strength gives a higher elastic modulus, resulting in lower camber values. Various models available for long-term camber estimation provide formulas to calculate age-adjusted concrete strength in order to accurately predict the camber. A lot of the studies in the past (Rosa et al. (2007), Rizkalla et al. (2011), O'Neill and French (2012)) illustrate that the strengths of concrete at release were underpredicted when using the existing camber prediction models. To solve this problem, various researchers suggest using different multipliers to account for the underpredicted concrete strength at release.

2.2.2. Elastic Modulus

The modulus of elasticity is a significant variable in prestressed concrete because it affects the instantaneous and long-term camber. It is interdependent with the concrete compressive strength. As discussed in the previous section, the concrete strength will

affect the modulus of elasticity and subsequently affect the camber. Thus, the method of calculating the elastic modulus should consider the concrete strength development with age to account for the time-dependent effects.

Jayaseelan and Russell (2007) examines the effect of changing the elastic modulus by $\pm 20\%$ and its effect on camber. Rosa et al. (2007), Rizkalla et al. (2011), O'Neill & French (2012) and Mante et al. (2019) found that the general equations for the calculation of elastic modulus generally underpredict its value and hence overpredict the camber. Based on these studies, the authors recommend calibrating the existing models to reflect the characteristics of the regional materials and corresponding modulus of elasticity of concrete.

2.2.3. Creep

Long-term camber and deflections are significantly affected by creep and shrinkage of concrete. When loaded, the concrete deforms elastically initially and will continue to deform with the passage of time. Even if the load is removed, the total deformation is only partially recoverable. This continued deformation is called creep. The creep deflection is calculated by multiplying the creep coefficients by the corresponding elastic deflections.

2.2.4. Shrinkage

During the drying process, volume of the concrete decreases and causes the beam to decrease in length. This contributes to prestress losses, which in turn results in decreased beam camber with time. Thus, the prediction of shrinkage strain to be experienced by the girder is significant.

2.2.5. Losses

The reduction in the initial prestressing force during the life of a girder is called the prestress loss. The total losses are the collective result of instantaneous losses and time-dependent losses. The instantaneous loss is due to the elastic shortening of the member while the combination of creep and shrinkage losses and the relaxation of prestressing steel are included in the time dependent losses.

During the transfer of the prestress, the axial compressive force applied to the girder causes shortening and elastic bending. The bond between the prestressing steel and concrete causes the strands to shorten, reducing the tension stress and strain.

The reduction in prestressing force with time when held at a constant length is called Relaxation of steel. It is dependent on several variables, including the initial force, the properties of steel, and the temperature of the prestressing strands.

2.2.6. Other factors

Shrinkage and creep are influenced by aggregate properties, cement hydration characteristics, duration of curing, age of loading, and ambient humidity (Gardener and Lockman, 2001). Gilbertson and Ahlborn (2004) found strength of concrete at release, initial strand stress and strand eccentricity to affect the prestress losses most.

The locations of supports underneath the prestressed concrete beams during storage can vary from beam to beam by a few feet (Honarvar et al., 2015). The overhang of the supports reduces the length of the beam and affects the camber as shown in Figure 2-1. Beams which are stored differently will have varied overhang lengths and thus will result in significant camber variability. Tadros et al. (2011) and Honarvar et al. (2015)

studied the influence of the storage duration and conditions and recommended that these factors should be accounted for in the prediction of at-erection camber.

Rizkalla et al. (2011) observed that the temperature fluctuations of the strands have a significant impact of the stress reduction of steel, and hence on the camber. O'Neill & French (2012) considered the additional prestress losses due to the relaxation and thermal effects in the calculation of the camber.

Honarvar et al. (2015) instrumented the prestressed beams with potentiometers and thermocouples to monitor the effect of temperature changes on deflections over a 24-hour period. Long-term camber variation of as much as 0.75 in. (19.0 mm) was observed. The individual errors associated with inaccurate measurement of the instantaneous camber in field due to deflections and friction of the bed, and irregular surface on the top flange may be small, but the combined effect of all these errors can cause a large discrepancy between the measured and designed camber.

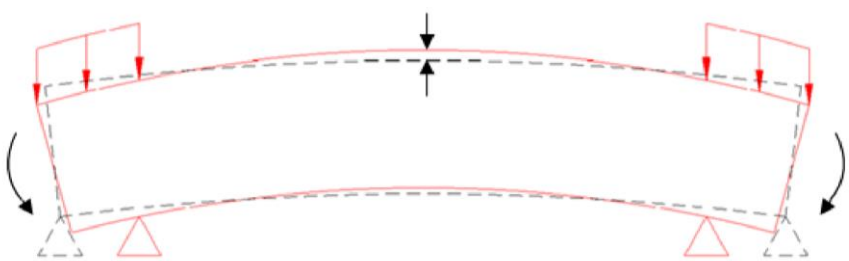

Figure 2-1: Prestressed concrete beam with increased midspan deflection caused due to overhang (Reprinted from Honarvar et al., 2015)

2.3. Previous Work and Comparison of Models

Accurate camber prediction in prestressed concrete bridge beams is critical to all parties involved in bridge design and construction. The models for estimation of prestress losses

available presently differ from each other in their ability to incorporate material properties, time increments, and prestress losses. Many commonly used models or methods for prestress loss prediction and accurate estimation of camber, were formulated many years ago or are developed using approximations that do not entirely match what is seen in current practice. As higher strength concrete becomes more practical for design, the spacing between beams becomes wider, and longer spans can be achieved. There is some question as to whether the current models still apply, or if the results are being extrapolated beyond an acceptable limit. This poses a question as to which are the appropriate models that can be used to accurately predict the camber in the present time.

Martin (1977) presents a rational method for estimating long-term multipliers for deflection and camber of prestressed concrete girders for each stage of construction. The paper follows a series of stages for topped and untopped precast prestressed concrete members and their long-term multiplier estimation. It takes into consideration the various factors related to the construction of prestressed members like concrete mix, time of release of prestress, erection time and time of application of superimposed loads, etc., and can accurately predict the long-term deflection and camber except for extremely long spans. A sensitivity analysis is also presented by changing one variable at a time. Some very general assumptions were made to develop these multipliers.

These include:

- Basic time-dependent factor: 2.0
- Time-Dependent loss of prestress: 15%
- Age of Erection: 40 - 60 days

- Total camber/deflection change at erection: 50%
- Ratio of I_0/I_c: 0.65

Table 2-1: Suggested multipliers to be used as a guide in estimating long-time camber and deflections for typical members (Reprinted from Martin 1977)

		Without Composite Topping	With Composite Topping
	At erection:		
(1)	Deflection (downward) component – apply to the elastic deflection due to the member weight at release of prestress	1.85	1.85
(2)	Camber (upward) component – apply to the elastic camber due to prestress at the time of release of prestress	1.80	1.80
	Final:		
(3)	Deflection (downward) component – apply to deflection calculated in (1) above.	2.70	2.40
(4)	Camber (upward) component – apply to camber calculated in (2) above.	2.45	2.20
(5)	Deflection (downward) – apply to elastic deflection due to super-imposed dead load only	3.00	3.00
(6)	Deflection (downward) – apply to elastic deflection caused by the composite topping	-	2.30

Gardner & Lockman (2001) uses the information available at design, to present a design-office procedure for calculating the shrinkage and creep of for concretes with mean compressive strengths less than 82 MPa (11.9 ksi). This design information includes the specified design concrete strength, the strength of concrete at loading, relative humidity and the size of element. The simple design-office procedure is a compromise between completeness and simplicity, hence the number of parameters that can be used are limited.

The method includes time-dependent strength development and the corresponding elastic modulus, and equations to predict creep and shrinkage. The method does not require any other input parameter like the type of chemical admixtures or mineral by-products in the concrete, the casting temperature, or the curing regime. Aggregate stiffness is also taken into account by back-calculating it from the measured modulus of elasticity of the concrete. The shrinkage term K can be estimated from measured strength gain, regardless of the cementitious ingredients in the mixture. Experimental results for 185 sets for long-term camber and 115 sets for shrinkage indicate creep and shrinkage can be estimated within ±30%. The experimental data is also compared with the results using ACI 209, CEB MC1990, and B3.

Gilbertson & Ahlborn (2004) uses various prediction methods to estimate the prestress loss at final service conditions for two typical bridge systems. It was seen that the variations in material of concrete and steel, geometric characteristics of the bridge, and variable environmental factors lead to large discrepancies in prestress losses and subsequent camber and deflection predictions. The authors found jacking stress, compressive strength of concrete at strand release, relative humidity, and eccentricity of strand as the primary influencing factors.

Hinkle (2006) examines some of the commonly used methods of predicting camber of prestressed concrete beams and verify their accuracy in predicting the camber of actual beams. Two general types of prediction methods are discussed – multiplier methods and an incremental time step method. Prediction equations for concrete modulus of elasticity are also compared with experimental results from test cylinders made from

the concrete mix used to fabricate the studied beam. The variability of calculated camber using the measured and predicted modulus of elasticity is examined. 27 Modified AASHTO bulb tee beams having design strength as 9 ksi were investigated for spans between 127 ft to 138 ft. Camber measurements were taken at weekly intervals until the beams were one month old, after which time the measurements were decreased to monthly intervals. Differences in measured camber for beams cast in different seasons, spring and summer, are examined. The creep, shrinkage, and elastic modulus calculated using Shams and Kahn model resulted in the most accurate predicted beam deflections when used in combination with the incremental time step method. The GL-2000 and AASHTO-LRFD models were also observed to lead to similarly accurate overall predicted beam deflections. Camber predicted by the PCI Multiplier Method based on Martin (1977) was 48% greater than the measured beam camber at the assumed beam setting age of 60 days. A seasonal difference in compressive strength was observed, with summer compressive strength being lower than winter compressive strength for the same mix design.

Jayaseelan & Russell (2007) reviewed literature on existing methods for prediction of prestress loss and related research and conducted a parametric study of various factors affecting camber. The studied parameters included varying the modulus of elasticity and the creep coefficient by +/- 20% and varying the design properties like adding prestressing strands at top flange, adding mild steel at midspan in the bottom flange. The results were analyzed using PCI multiplier method, 2010 method, the AASHTO LRFD Refined Losses method, the NCHRP 496 Detailed Prestress Losses method and the AASHTO LRFD Time Step method. Sensitivity analysis was conducted by varying each parameter at once. The

long-term camber was reduced by almost 7% on decreasing the creep coefficient by 20% and by 12% when concrete elastic modulus was increased by 20%. Additionally, the AASHTO LRFD Time Step method was recommended over the other methods since it is formulated for High-Performance Concrete and accounts for the variability in the material properties. While the reduction in camber was approximately 10% and 17.4% due to the addition of (4) #7 and (5) #9 mild steel bars respectively, the addition of two and four prestressing strands was found to reduce the camber by 35% and 69% respectively. Therefore, the authors recommend adding prestressing strands at top and/or mild steel at midspan in bottom flange in order to prevent excessive long-term camber.

Rosa et al. (2007) used material testing and field measurements to calibrate the existing predictive models. Adjustment factors were proposed based on actual compressive strength, elastic modulus and concrete creep and shrinkage of the material and observed camber in field. Fabricator data was also collected for girders varying in shape, length, and strand arrangement. Girders were also monitored for the effects of varying age of loading and support conditions on camber. The authors found that the measured concrete strength at release was on average, 10% higher than the designed concrete strength and the concrete elastic modulus was 15% higher than predicted by the AASHTO LRFD equation. Based on these results, an adjustment factor of 1.15 was proposed for the elastic modulus and a factor of 1.4 was proposed for the creep coefficient when using the AASHTO LRFD model. Ultimately a program was developed to help the users create improved camber predictions by allowing them to input properties of concrete produced from local materials. The observations from actual camber data showed that the

AASHTO 2006 model provided much better estimates for the prestress losses than the 2004 model, which was the commonly used model by WSDOT for camber prediction.

Rizkalla et al. (2011) evaluated the effect of production factors like debonding and transfer length, temperature, curing method and other important factors like concrete compressive strength, project scheduling on the prestressing camber of various girder shapes. Adjustment factors of 1.25 for the release design concrete strength and 1.45 for the 28-day design concrete strength were proposed in order to better predict the long-term camber for prestressed concrete beams. The modulus of elasticity of concrete calculated using AASHTO LRFD (2010) model was found to be 15% higher than the actual results. It was also observed that the temperature fluctuations of the strands have a significant impact of the stress reduction of steel, and hence on the camber. The resulting stress reduction in steel is about 7%, which is outside the industry tolerance of 5%. Differential cambers were observed in identical girders because of difference in storage durations and project phasing. The moist cured members were observed to have higher camber at time of transfer of prestress than the steam cured members. A detailed method using multipliers for simplicity and an approximate method using time-dependent losses and creep factors for more accurate camber prediction are proposed. The current method used by NCDOT was also revised to incorporate the effect of the factors related to girder production. Cambers calculated using the current NCDOT method, the modified NCDOT method, and the two proposed methods were compared with measured cambers of 382 prestressed concrete girders in the field. With the new proposed methods, the predicted camber was within 10% of the actual camber.

Tadros et al. (2011) proposes a method to develop spreadsheets for including AASHTO prediction formulas to predict initial and long-term camber and investigates camber variability. Modulus of elasticity of concrete calculated using two different models - AASHTO LRFD 2007 and ACI 363 2010 was found to cause large variance in camber (±22%). Thus, the authors recommend using historical records of the measured concrete elastic moduli at precasting plants that supply prestressed girders. Even though the effects of higher concrete strengths at release, length of curing and difference in temperature with beam depth were recognized, these effects were not studied in detail. The effect of erection age of girders is also seen to produce camber variability in girders produced from the same batch and having same storage conditions. The proposed equation to estimate deflection due to the self-weight of the girder also accounts for the effect of the overhanging ends of the beam during storage. To account for the camber variability, the authors suggest that a haunch of at least 2.5 in (63.5 mm) should be assumed during the design of girder. Finally, the authors also recommend that the girder seats should be finalized only around the time of erection to allow for camber measurements to be taken before shipping.

O'Neill & French (2012) observed that the primary reasons for lower field camber at release than predicted were underpredicted concrete strengths at release (average 15.5% and some as high as 35%), underpredicted elastic modulus, and unaccounted thermal prestress in design. Adjustment factors of 1.15 for the release design concrete strength and using AASHTO LRFD specifications for the elastic modulus prediction were proposed in order to better predict the long-term camber for prestressed concrete beams. ACI 209R-92 was used to predict creep and shrinkage losses. Historical data for 1067 girders was

collected and analyzed. Various time-dependent factors' influence like solar radiation, relative humidity, thermal effect on prestress losses, concrete creep and shrinkage, duration of curing and conditions of storage on long-term camber was also investigated. The observations support that the variation in age of girder at erection causes camber variability. The camber of girders would show approximately +-10% difference if the erection age is 30 and 365 days respectively. Therefore, the authors recommend using more than one multiplier for different average ages of erection. Minor increase in camber was observed due to high relative humidity in the winter months. Weekend curing results in cooler concrete temperatures which in turn reduces the thermal prestress losses. The authors also found that when stored, the girders had large overhangs (>L/15) which additionally caused camber variability if stored for more than 300 days. Because the time period between strand pull and strand release varied from ~1 to 6 days, the stress loss due to relaxation varied from 1.8 ksi to 2.7 ksi (Table 2-2). The report recommends using a typical relaxation loss to be approximately 1.1% of the initial pull stress based on the assumption that most commonly, the strands are tensioned for 2 to 3 days before releasing.

Table 2-2: Strand stress losses due to relaxation (Reprinted from O'Neill & French, 2012)

Time between pull and release (days)	**1**	**2**	**3**	**4**	**5**	**6**
Stress loss (ksi)	1.76	2.13	2.35	2.50	2.62	2.71

Table 2-3: Impact of higher strength of concrete at release on design camber (Reprinted from O'Neill & French, 2012)

% Increase in concrete strength	% of design camber
5	98.4
10	97.0
15	95.5
20	94.2
25	92.1
30	91.7
35	90.6

Table 2-4: Camber results for weekday vs. weekend cure (Reprinted from O'Neill & French, 2012)

Bridge #	Weekday cure	Weekend cure	% Difference
17532	0.967	0.859	12.7
01531	0.914	0.846	8.1
19561	0.905	0.888	1.9
27R20,21	0.930	0.872	6.6
19850	0.767	0.736	4.3
14816	0.755	0.759	-0.5
07581	0.735	0.720	2.2
72013	0.712	0.680	4.6
69844	0.810	0.700	15.8
14549	0.857	0.809	6.0
Total	-	-	6.2

Table 2-5: Multipliers for at-erection camber prediction (Reprinted from O'Neill & French, 2012)

Girder Age at Erection	Mn DOT multiplier	Improved multiplier
0-60 days	1.25	1.65
61-180 days	1.40	1.85
181-365 days	1.50	2.00
366+ days	1.55	2.05

MnDOT Single Multiplier: 1.35
Improved Single Multiplier: 1.80

Kamatchi et al. (2014) evaluates the different models available for prediction of long-term camber and prestress losses, taking into account the effect of shrinkage, creep and prestress relaxation. Four commonly used models—ACI 209R-92, B3, CEB MC90-99, and GL2000 have been utilized to estimate long-term creep and shrinkage and compare the results of the theoretical analysis with the field measurements. The paper attempts at identifying the suitable time-dependent creep coefficient and shrinkage strain models to estimate the long-term prestress losses and camber for an existing box-girder bridge span. It was found out that the ACI 209R.08 and CEB MC90-99 models usually underestimate and GL2000 and B3 models overestimate the camber predictions (Figure 2-2). Based on the studies, the authors recommend using the B3 model for estimation of camber for the initial 5 years after prestress member construction, and the CEB MC90-99 model for estimation of long-term camber. However, it was found that ACI 209R-92 model predicts closer prestress losses with experimental measurements for prestressed concrete beam.

Honarvar et al. (2015) describes the commonly faced problems faced by Iowa DOT. It was observed that Martin's multipliers, which is the commonly used procedure

by Iowa DOT to predict the long-term camber and deflection tends to overpredict the deflection of long span beams and underpredict the short span beams. Furthermore, differential camber was observed on beams cast on the same bed. This report monitors the dependency of camber on the elastic modulus, prestressing force and its losses, transfer length, storage conditions and temperature gradient on instantaneous camber prediction.

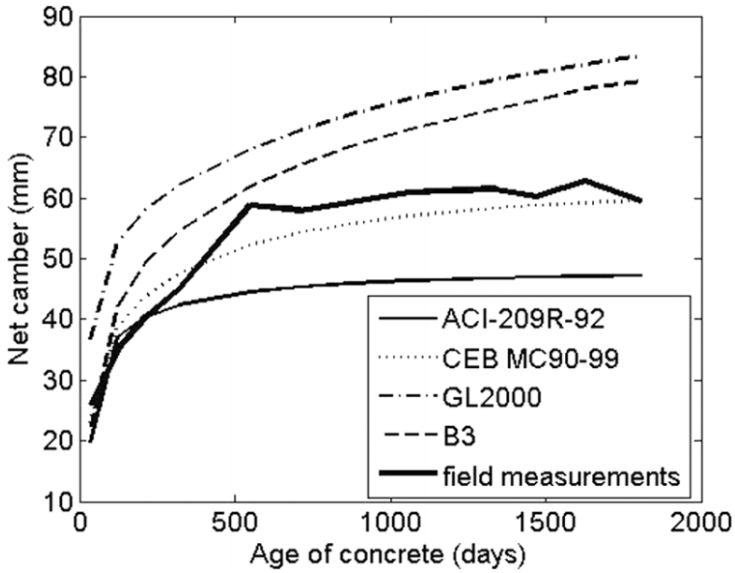

Figure 2-2: Comparison of long-term midspan camber with field measurements (Reprinted from Kamatchi et al., 2014)

It was observed from the results that the AASHTO LRFD (2010) recommendation for estimating the elastic modulus provided 98% ± 15% agreement with the measured instantaneous cambers. The results also indicated that the concrete strengths at release were typically underestimated (39.5% and 11.5% higher when designed concrete strengths were between 4.5 to 5.5 ksi and 6 to 8 ksi respectively), which caused an underprediction in the elastic modulus and subsequently an overprediction in the observed camber. Hence, to obtain the 28-day concrete strength, an average multiplier of 1.4 for designed concrete strengths 4.5 to 5.5 ksi and 1.1 for designed concrete strength 6 to 8 ksi is recommended

where experimental data is not available. The temperature gradients over a 24-hour period were seen to cause as much as 0.75 in. variations in camber. The prestressed beams stored at the precast plants exhibited an overhang length of Span/30 on average. Simplified and numerical analyses as well as finite element analyses were carried out to study the variation in camber from transfer of prestress to time of erection and long-term. The finite element analysis for the instantaneous camber proved to be in agreement with the field measurements.

The authors recommend a set of time dependent multiplier for different average erection lengths with and without overhang (Table 2-6, 2-7, 2-8 and 2-9). A single multiplier with and without the effect of overhang is also proposed for simplified analysis. The effect of thermal effect is also accounted for by considering a temperature multiplier, λT. The use of recommended multipliers to estimate the long-term deflection can improve the accuracy compared to the existing Iowa DOT approach. The accuracy of camber predicted using proposed multipliers was higher when the prestressed beams had no overhang during storage.

Table 2-6: Recommended single multipliers for at-erection camber prediction without overhang during storage (Reprinted from Honarvar et al., 2015)

Group	Average time (days)	Multiplier
Large Beams	120	1.41
Small Beams	120	1.57

Table 2-7: Recommended single multipliers for at-erection camber prediction with L/30 overhang during storage (Reprinted from Honarvar et al., 2015)

Group	Average time (days)	Multiplier
Large Beams	120	1.61
Small Beams	120	1.86

Table 2-8: Recommended set of multipliers for at-erection camber prediction without overhang during storage (Reprinted from Honarvar et al., 2015)

Erection Period (days)	Group	Average time (days)	Multiplier
0-60	Large Beams	40	1.35 ± 0.01
	Small Beams	40	1.53 ± 0.02
60-180	Large Beams	120	1.41 ± 0.02
	Small Beams	120	1.61 ± 0.02
180-480	Large Beams	310	1.46 ± 0.02
	Small Beams	300	1.67 ± 0.02

Table 2-9: Recommended set of multipliers for at-erection camber prediction with L/30 overhang during storage (Reprinted from Honarvar et al., 2015)

Erection Period (days)	Group	Average time (days)	Multiplier
0-60	Large Beams	45	1.55 ± 0.02
	Small Beams	45	1.77 ± 0.02
60-180	Large Beams	115	1.61 ± 0.02
	Small Beams	120	1.86 ± 0.03
180-480	Large Beams	320	1.68 ± 0.02
	Small Beams	340	1.94 ± 0.02

Lee et al. (2018) states the limitations of the simplified multiplier method (Martin 1977, PCI 2010) and develops new multipliers which considers various construction processes and has characteristics for the modern girder sections and topping thicknesses. The current PCI multipliers method do not consider the construction planning and schedule and can predict the long-term camber only at erection and final. Also, the multipliers considered for the composite cross-section are not consistent with the cross-section characteristics seen in current prestressed concrete bridges. The long-term deflection prediction results using the proposed multipliers were compared with those using the basic PCI single multiplier method, modified PCI, ACI 318-14 and numerical analysis. It is found that using the newly proposed method can better predict the long-term behavior at any given time after casting. The new proposed modified PCI multipliers are based on the rate of shrinkage and creep over the passage of time. The predictions using the newly proposed multipliers showed similar results as that of the numerical analysis results.

Based on the studies conducted on nine normal weight girder production cycles, Mante et al. (2019) suggests calibrating the prediction models for regional concrete material properties like strength of concrete, elastic modulus and creep and shrinkage. Once calibrated, these prediction models are seen to reduce the overprediction to nearly 10 percent from the usual 50 to 68 percent overprediction generally observed in existing construction on field. The author also suggests using an elastic modulus prediction equation that accounts correction factors for aggregate properties along with a model

which uses time-step increments for analysis such as *fib* Model Code (2010) or AASHTO LRFD to predict creep and shrinkage.

2.3.1. Summary

The past studies indicate that the primary source of errors in the prediction of camber and deflection of prestressed concrete beams were the inaccurate estimations of the material properties of concrete, like the concrete strength, modulus of elasticity, creep and shrinkage and the magnitude of prestressing force. The underprediction of concrete strengths by the models causes the elastic modulus to be underestimated, leading to overprediction in camber. Thus, the studies suggest that the models should be adjusted according to the properties of the local materials. According to Naaman (2004), all the models for predicting camber primarily use the same method of calculating instantaneous losses even though their procedures may vary to determine the long-term prestress losses. The difference in the values of instantaneous losses when calculated using different models occur because of the variation in concrete and steel properties considered for the analysis. Many studies (Hinkle, 2006), (Jayaseelan & Russell, 2007), (Rosa et al., 2007), (Rizkalla et al., 2011), (O'Neill & French, 2012) illustrated that the refined method of predicting prestress losses provided by AASHTO LRFD can give a good estimation of the camber of prestressed concrete beams. Coefficients of creep and shrinkage obtained from the models were validated only by Gardner & Lockman (2001), Rosa et al. (2007), and Honarvar et al. (2015).

Table 2-10: Multipliers for concrete strength proposed by previous researchers

Reference	Release multiplier for concrete design strength	Long-term multiplier for concrete design strength
Rosa et al. (2007)	1.10	1.25
Rizkalla et al. (2011)	1.25	1.45
O'Neill & French, 2012	1.15	-
Honarvar et al. (2015)	1.4 for 4.5-5.5 ksi 1.1 for 6-8 ksi	-

Table 2-11: Comparison of considered parameters for existing camber prediction models

Considered Parameters	ACI 209R-92	*fib* 2010	AASHTO LRFD (2017)
f'_c, ksi	-	2.9 to 13	Up to 15
Cement content	$470\ to\ 752\ lb/yd^3$	-	-
Relative humidity %	40 to 100	40 to 100	35 to 100
Type of cement	I or III	I, II, III	I, II, III
Age of steam curing before loading	1 to 3 days	1 to 3 days	1 to 3 days
Age of moist curing before loading	7 days	<=14 days	7 days
Age of loading	≥1 day	≥1 days	≥1 day
Air content	≤6%		
Slump	2.7 in.		
Size effect	Considered	Considered	Considered
Fine aggregate	50%		
Moist curing temperature	73.4 ± 4°F		
Steam curing temperature	≤ 212°F		

3. UNTOPPED PRESTRESSED CONCRETE GIRDERS

3.1. Introduction

The concept of load balancing for prestressed concrete was first introduced by T.Y. Lin (Lin, 1995) for both simply supported and continuous (indeterminant) structures some 60 years ago. This load balancing concept achieved using draped parabolic post tensioned (PT) tendons is the most effective approach for prestressed girder construction. However, it is often neither expedient nor economical to use PT for individual girders. Pretensioning is generally the economic solution for precast portions of a structure. While its effective to balance most of the dead load, this approach can cause rider discomfort if the deflections are not properly accounted for by the design. Generally, these deflections are dealt with during the construction by providing variable depth haunches to form the deck slab. The general idea for the design of pretensioned concrete girders is minimizing the prestressing force by maximizing eccentricity. This leaves end moments that lead to hogging after the units are precast. Some limited sagging will take place as the prestress losses continue to develop over time. It is likely that a net upward deflection will remain after all losses are complete. Hence, along with the load balancing concept, it is proposed that a deflection balancing concept also needs to be used when building a complex bridge system.

For long span girders, deflection control becomes a major governing feature as large deflections in the bridges does not allow a smooth ride to the rider. By changing the number and arrangement of prestressing strands, deflection may be easily controlled. Harping further improves critical conditions where straight tendon profile fails to keep deflection under check.

The aim after completion is to ensure the deck profile of a prestressed concrete girder, topped with a uniform thickness slab is as flat as practical (after long term losses).

The order of objectives is:

i. Minimize overall deflections under self-weight to achieve the best possible ride quality

ii. Minimize the force after losses

In this chapter, it is demonstrated how straight and harped pretensioned prestress untopped systems may be designed to minimize deflection under girder self-weight. The concept of deflection balancing is introduced, and the associated near optimum prestress design is formulated. Prototype bridge geometries are designed using the concept for the unshored method of construction. The design examples are developed for both eccentric and harped tendon profiles using their respective near optimum relations between force, eccentricity and the harping distance. Application examples based on minimal force prestressing design are also formulated and the deflections are compared with the deflections of design based on optimized prestress solutions.

3.2. Deflection balancing solutions for non-composite system

The objective of prestressed concrete member design is to ensure that the stresses are within permissible limits, and the deflections are disregarded by design but are instead dealt with during construction. In case of a simply supported beam, the best approach to perfectly balance loads and negate dead load deflections, is to drape the post-tensioned tendons in a parabolic form. But for a pretensioned system, only one of these objectives can be achieved with either straight or harped strands. Harped pretensioning may partially

balance the dead load as well as deflection. This causes the pretensioned girders to camber upward, which are later dealt with by using variable depth haunches to form the deck slab.

Using a magnel diagram approach, equations for the force (F) after losses (such that $F = 0.8F_i$; where F_i = force at transfer) and the associated eccentricity are developed to keep the stresses within permissible limits. Along with stress governing equations, an equation that minimizes deflection is also included.

A general relation between force and eccentricity of the pretensioned prestress strands is defined as:

$$Fe_0 = \gamma_0 WL \tag{3-1}$$

$$Fe_c = \gamma_c WL \tag{3-2}$$

where, $F =$ force after losses; $e_0 =$ eccentricity at beam ends; $e_c =$ eccentricity of prestressing steel at center with respect to the C.G. of the concrete section; $W =$ total weight of the girder; $L =$ span of the girder; and γ_0 , $\gamma_c =$ deflection balancing coefficients at end and at midspan respectively.

Figure 3-1(a) and 3-1(b) represents the force after losses required per WL/e_c and the end eccentricity with respect to the midspan eccentricity respectively, and the horizontal axis denotes the harping coefficient, α normalized with respect to the length of the beam. The deflection profiles for the contrasting prestressing approaches for the simply supported beam under dead load alone are presented in Figure 3-1(c); the vertical axis is normalized to the deflection of a fixed-fixed simply supported beam ($\frac{WL^3}{384EI}$).

3.2.1. Eccentric prestress solution

This type of solution is the most common type of pretensioning system since it is the cheapest to manufacture. A solution $Fe_c = WL\ /\ 10$ is adopted herein as the reference for comparison for different prestressing solutions since it balances 80% of the self-weight and deflection. The prestress tendon profile is straight, i.e., the center and end eccentricity are same.

The first point in the Figures 3-1(a) and 3-1(c) represent the eccentric solution when the deflections are minimized and the difference of maximum and minimum observed values of deflections are zero. For this solution, the eccentricity is set to $Fe_c = WL\ /\ 9.9$ ($\gamma_0 = \gamma_c = 0.101$). The resulting maximum deflection is reduced by 14% of the reference with the increase of only 0.6% in the force if the center eccentricity is assumed to be same. This solution provides the best possible result with respect to deflection balancing when an eccentric only solution is used.

3.2.2. Harped solution with no end eccentricity

This prestressing system gives the solution as close to the parabolic profile. The least deflection using a harped profile with zero end eccentricity is found when the strands are anchored at $0.305L$, but it may sometimes be impractical to achieve such precision on field. Hence the value of $0.3L$ with $Fe_c = 0.1180WL$ gives a near optimum and practical minimum theoretical deflection solution. The resulting maximum deflection is reduced by 93% with only 18% increase in the force. For practical purposes, the harping point may be taken as $0.33L$. This is also a good solution if $Fe_c = 0.1227WL$. In this case, the deflection is reduced by 89% with 23% increase in force. For $\alpha < 0.3$, the deflection is not

minimized and for α > 0.33, the force required to minimize the deflection is significantly higher than the reference force. Therefore, the recommended α values when using a harped only profile are 0.3 and 0.333. It is evident that $0.3L$ gives the theoretical minimum deflections along with lesser prestress force, while 0.33 gives a more practical construction approach with slightly higher prestress force and deflections when compared to the $0.3L$ case.

3.2.3. Harped solution with some end eccentricity

It is not always possible to achieve a pure harped solution, and an eccentric only solution is not very effective in minimizing the deflections. Hence a mixed solution is preferable which is basically a harped solution with some end eccentricity. For this solution, two variables may be adjusted (γ_0 and γ_c) for a certain harp point (α), many viable mixed solutions are possible. The end eccentricity is assumed to lie between the kern points of the beam $(d/6)$; and the center eccentricity is assumed to be nearly $0.4d$. The minimum deflection is obtained for the harp point at $0.349L$, but it is rounded to $0.35L$ to increase construction practicality. For $\alpha = 0.35$, the deflection is reduced by 98% when $Fe_0 = 0.0162WL$ and $Fe_c = 0.1212WL$. The force is 21% more than the reference force. This solution may be adopted as the best pretensioned alternative of using parabolic draped PT tendons. But the solution for α = 0.33 with $Fe_0 = 0.0116WL$ and $Fe_c = 0.1201WL$ would be a more practical solution for construction. This gives the deflection 4% of the reference with only 20% increase in force if the center eccentricity is assumed to be same for all the cases.

3.2.4. Load balancing solutions

The solutions proposed in the previous sections give near minimum deflections, but they do not necessarily balance all the dead load on the beam. To achieve the dual objective of minimizing the deflections and also balancing the dead load, the Fe_c may be set to 0.125 (WL/8). For simplicity in calculations, the center deflection may be equated to zero. Doing this gives a relation between the end and center eccentricity for the chosen harp point. This relation can be used in the design process to achieve a nearly flat deck profile which also balances all the dead load on the beam. A load balancing ensures a perfectly rectangular stress block without any bending stresses under the combined effect of prestress and dead load.

This method gives higher deflections for $\alpha < 0.3$, but gives optimum results as the harping points are moved closer to the midspan. To achieve minimum deflection if the midspan moment is to be balanced, then α = 0.4 (Figure 3-1(d)) is recommended. The resulting deflection is reduced by 93% compared to the reference with 25% increase in prestressing force. Though this method does not give the theoretical minimum deflections, the method allows the engineers to find optimum relations in a simplified form, without many calculations or assumptions. The resulting deflections are also within the industry tolerances and can still improve the serviceability and rider comfort when compared with the current practices.

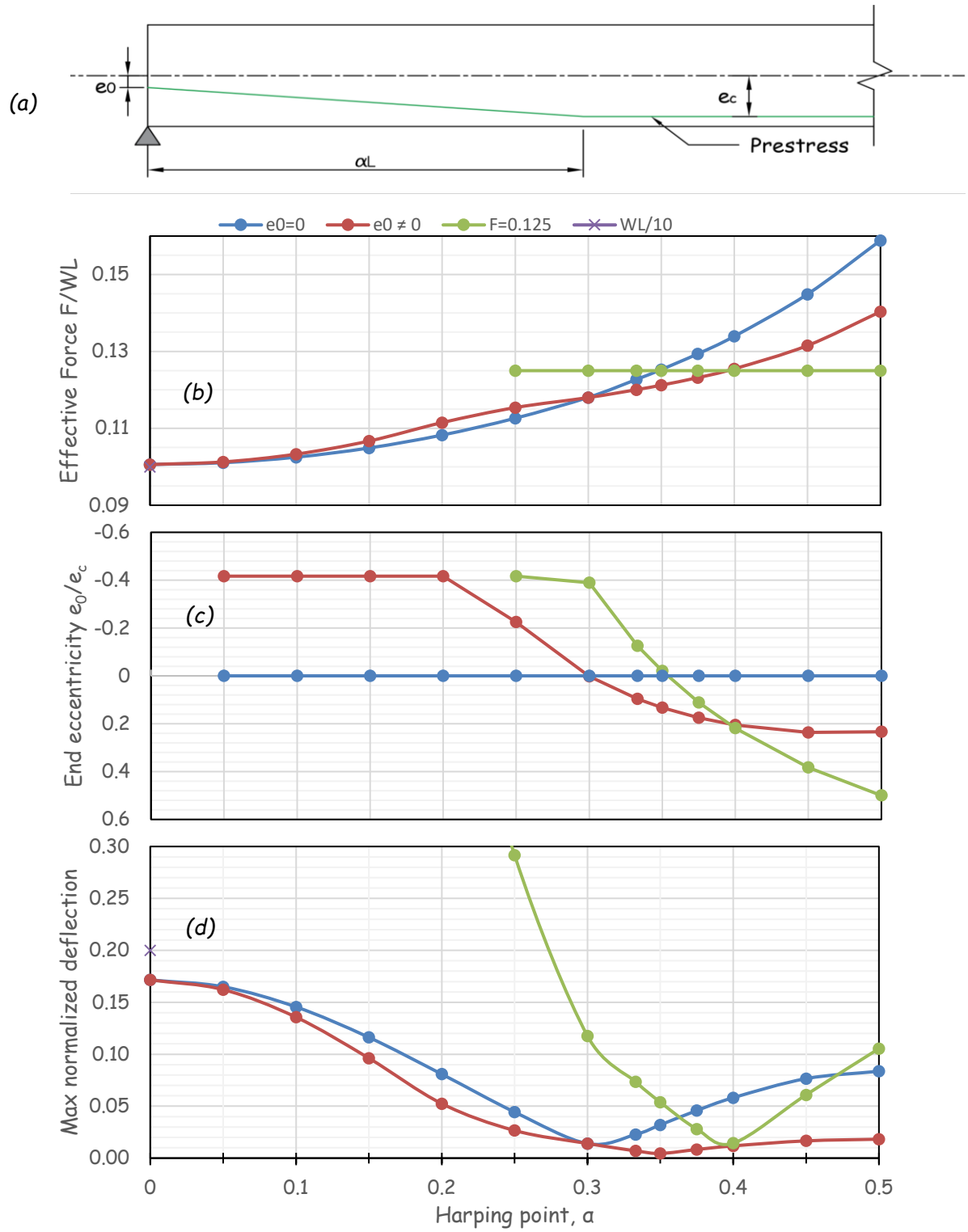

Figure 3-1: Deflection outcomes when deflections are minimized: (a) Applied prestress after losses; (b) end eccentricity with respect to midspan eccentricity; and (c) resulting maximum deflection

Table 3-1 represents the recommended prestress solutions for different tendon layouts in order to minimize the long-term deflections for an untopped prestressed concrete bridge girder.

Table 3-1: Recommended solutions for minimum deflection

Prestress profile	Harp point, α	γ_c	γ_0
Eccentric	-	0.101	0.101
Harped with $e_0 = 0$	0.30	0.118	0
	0.33	0.123	0
Harped with $e_0 \neq 0$	0.33	0.120	0.012
	0.35	0.121	0.016
Load balancing	0.4	0.125	0.027

3.3. Long-Term Multipliers

To calculate the long-term deflections for the untopped (non-composite) section, the time-dependent properties of concrete and prestressing steel are taken into account and multipliers are multiplied to the initial deflection at release to obtain the final deflection. These multipliers are based on Martin's method (1977) which is also used in current practice and PCI Design Handbook (2010). These multipliers are given in Table 2-1. According to Martin (1977), the most common age of erection of girder is 40 to 60 days, where almost 50% long-term creep, shrinkage and losses have taken place. The instantaneous losses are assumed to be 5% of the total initial prestressing force while the long-term losses are assumed to be 15%. The final force after all the losses is assumed to be 80 percent of initial. Therefore, 87.5 percent of the initial force is assumed and a multiplier of 1.8 applied to the deflection and camber at release to obtain the net deflection

at erection. The multipliers for long-term are taken as 2.7 for the deflection of dead weight of girder and prestress at release and 3.0 for the superimposed dead load elastic deflection. The camber calculations at midspan using the multipliers for various stages of construction and service are given as follows:

1. Net deflection immediately after release of prestress:

$$\Delta_i = -0.95\Delta_{p,i} + \Delta_{g,i} \tag{3-3}$$

where $\Delta_{p,i}$ = deflection due to prestress only at transfer and $\Delta_{g,i}$ = deflection due to girder self-weight at transfer, in which,

$$\Delta_{p,i} = \frac{F_i e_{01} L^2}{8E_{c_i} I_0} + \frac{F(e_{c1} - e_{01})L^2}{6E_{c_i} I_0}\left(\frac{3}{4} - \alpha^2\right) \tag{3-4}$$

$$\Delta_{g,i} = \frac{5}{384}\frac{W_g L^3}{E_{c_i} I_0} \tag{3-5}$$

where F_i = initial prestressing force; e_{01} = eccentricity of the prestressing strands with respect to centroid of non-composite section at beam ends; e_{c1} = eccentricity of the prestressing strands with respect to centroid of non-composite section at center; L = length of the beam; E_{c_i} = elastic modulus of precast concrete at transfer ($E_{c_i} = 0.85E_c$); E_c = elastic modulus of concrete at 28 days; I_o = moment of inertia of the girder (non-composite section); W_g = total self-weight of the girder; and α = distance of beam end to the harp point.

2. Net deflection during erection at 40-60 days:

$$\Delta_e = -0.875\Delta_{p,i}(C_e) + \Delta_{g,i}(C_e) \tag{3-6}$$

where C_e = Multiplier for at-erection camber (From Table 2-1 (1)).

3. Net deflection immediately after addition of dead load (wearing surface):

$$\Delta_s = -0.875\Delta_{p,i}(C_e) + \Delta_{g,i}(C_e) + \Delta_{sidl} \tag{3-7}$$

in which Δ_{sidl} = deflection due to superimposed dead load (wearing surface) given by:

$$\Delta_{sidl} = \frac{5}{384}\frac{W_{sidl}L^3}{E_c I_0} \tag{3-8}$$

where W_{sidl} = total weight of the superimposed (added) dead load

4. Net long-term deflection under the effect of dead load and prestress:

$$\Delta_{LT} = -0.8\Delta_{p,i}(C_{LT-1}) + \Delta_{g,i}(C_{LT-1}) + \Delta_{sidl}(C_{LT-3}) \tag{3-9}$$

where C_{LT-1} = Multiplier for long-term deflection of precast concrete (From Table 2-1 (3)); and C_{LT-3} = Multiplier for long-term deflection of superimposed dead load (From Table 2-1 (5)).

3.4. Design Case for Eccentric and Harped profile

Two sets of application examples – each having eccentric only and harped tendon profiles for optimized prestress design and the minimal practical force design are developed and presented. These examples demonstrate the effect of using the proposed optimum relations on the long-term deflections of precast prestressed concrete girders for unshored method of construction. The design of the bridge is based on the provisions from AASHTO LRFD Bridge Design Specifications (AASHTO 2017) and the design parameters such as material properties of concrete and steel, and cross-sectional properties of the bridge are representative of typical values used in Texas.

3.4.1. Prototype Bridge Geometry and Girder cross-section

The geometry of the bridge is chosen based on the minimum stiffness required for the live load deflection according to AASHTO LRFD Bridge Design Specifications (AASHTO 2017) Article 2.5.2.6.2. A combination of uniformly distributed lane load and design truck loads is considered for the live load deflections. The lane loads and truck loads are multiplied by the number of lanes. Dynamic amplification factor of 1.33 is multiplied to the design truck load to compute deflections. Figure 3-2 shows the stiffness of the bridge based on the number of girders versus the stiffness (EI) required for different span lengths.

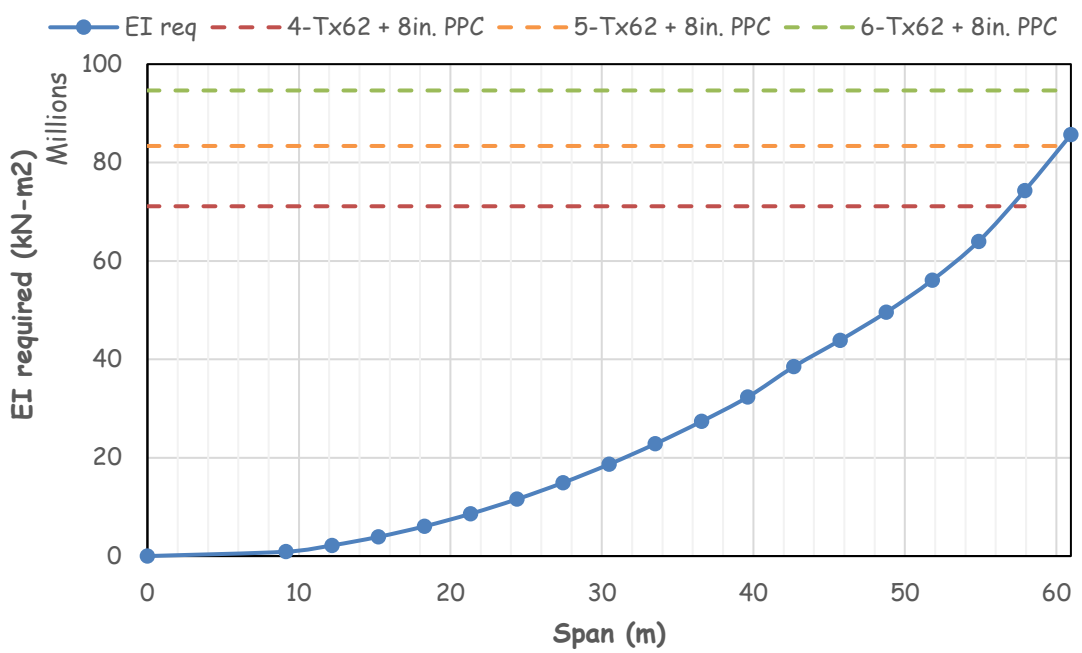

Figure 3-2: Minimum EI required for various span lengths

Figure 3-3 presents the geometry of the prototype bridge. The bridge deck cross-section is shown in Fig. 3-3(a). The bridge has a total width of 14 m with a standard barrier of 0.3 m width on each side. Therefore, the total roadway width of the bridge is 13.4 m.

The bridge superstructure consists of five modified Tx62 girders spaced at 2.9 m center-to-center with an overhang of 1.22 m on each side. A layer of asphalt as a wearing surface of thickness 51 mm is added onto the girder flanges. The asphalt surface does not contribute structurally, but adds dead load on the structure. A 2.44 m wide flange with a thickness of 203 mm is cast monolithically with a Tx62 girder to eliminate the need of a concrete deck topping. The flange width of 2.44 m is also chosen so as to satisfy the transportation limits. The splices of length 457 mm between the girders are filled with Ultra High-Performance Concrete (UHPC) and the mild steel #4 bars spaced at 203 mm o.c. are extended from adjacent flanges into the splices. Figure 3-3(b) represents the reinforcement in the splices. Figure 3-3(c) and (d) shows the details of the standard Tx62 girder and Tx62 with 203 mm monolithic flange.

Table 3-2 presents the uncracked elastic cross-section properties for the standard and modified Tx62 girder. The live load deflection is found to be 10 mm compared to the allowable limit of 38 mm specified by AASHTO.

3.4.2. Design Assumptions and Parameters

The prototype bridge designs are developed based on the design parameters and assumptions summarized in Table 3-3. These cross-sectional parameters and the material properties of concrete and steel were chosen based on the typical values generally adopted by TxDOT in accordance with the AASHTO LRFD Specifications (AASHTO 2017).

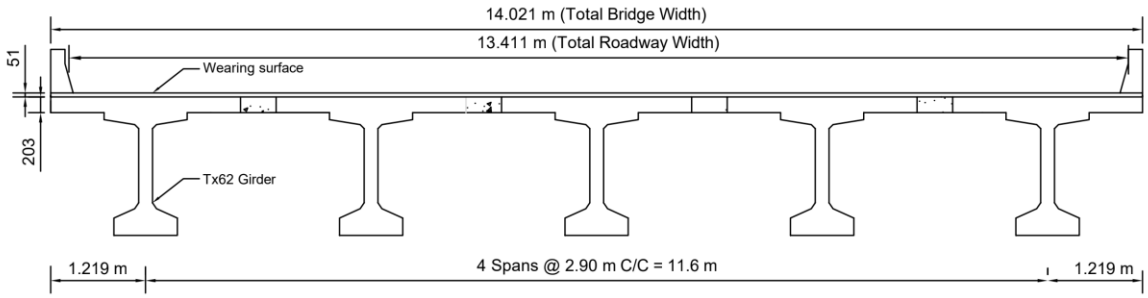

(a) Bridge deck cross-section

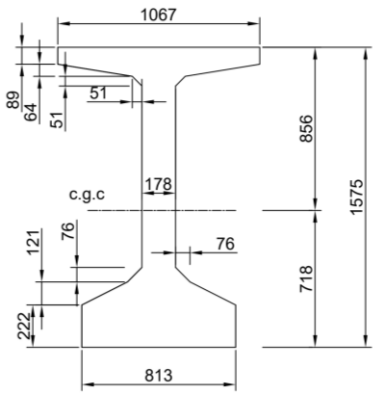

(b) Standard Tx62 girder

$A = 0.587\ m^2$

$I_x = 0.193\ m^4$

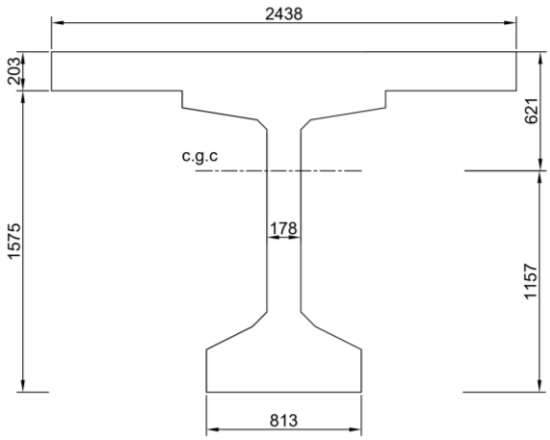

(c) Modified Tx62 with flange

$A = 1.083\ m^2$

$I_x = 0.441\ m^4$

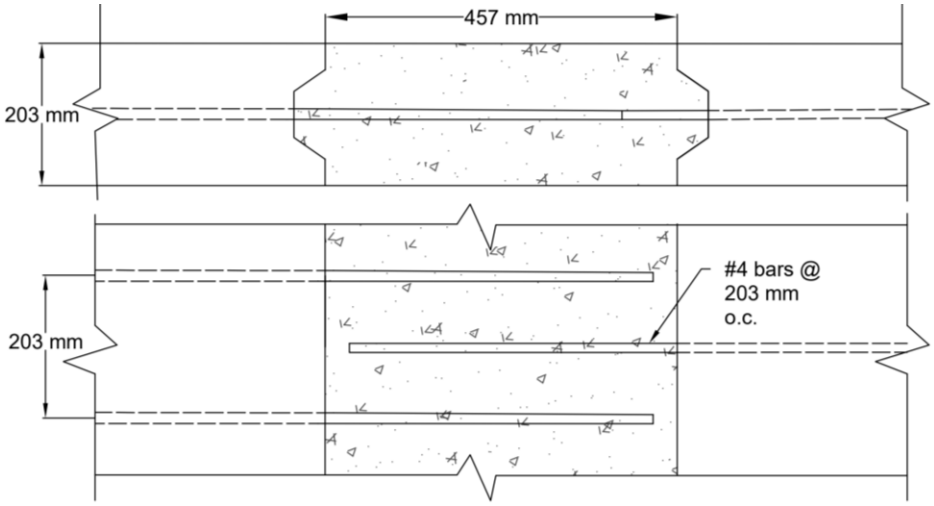

(d) Elevation (above) and Plan (below) view of splice connection

Figure 3-3: Prototype bridge cross-section for Untopped case

Table 3-2: Section properties for Untopped case

Section Property	Standard Tx62	Tx62 + 203 mm flange
Total height (mm)	1575	1778
Depth of N.A. from top of girder, y_t (mm)	856	621
Depth of N.A. from girder soffit, y_b (mm)	718	1157
Area, A (m^2)	0.587	1.083
Moment of Inertia, I_x (m^4)	0.193	0.441
Section Modulus, S_{xt} (m^3)	0.226	1.744
Section Modulus, S_{xb} (m^3)	0.269	0.936

Table 3-3: Bridge Design Parameters (Hueste et al., 2012)

Parameter		**Value**
Total bridge width		14.021 m
Unit weight of concrete (Precast), w_c		2400 kg/m^3
Unit weight of asphalt wearing surface, w_s		2243 kg/m^3
Precast Concrete Strength at release, f'_{ci}		42 MPa
Precast Concrete Strength at service, f'_c		60 MPa
Modulus of elasticity, E_c		36.23 GPa
Coefficient of Thermal Expansion of Concrete		$12 \times 10^{-6}/℃$
Relative Humidity		65%
Mild Steel	Yield Strength, f_y	414 MPa
	Modulus of Elasticity, E_s	200 GPa
Prestressing Steel	Strand diameter	15 mm
	Ultimate tensile strength, f_{pu}	1860 MPa
	Yield Strength, f_{py}	$0.9f_{pu}$
	Modulus of Elasticity, E_p	196 GPa
	Force per strand	146 kN
Pretensioning	Stress limit at transfer, f_{pi}	$f_{pi} \leq 0.75f_{pu}$
	Stress limit at service, f_{pe}	$f_{pe} \leq 0.8f_{py}$

The primary designs presented in this section are developed according to the state-of-the-art and practice of girder bridges. Following are the basic assumptions which are used for these primary designs (Hueste el al., 2012).

- The construction is assumed to be done using temporary intermediate diaphragms of structural steel shapes. The negligible weight of these temporary components is not considered in the calculations.
- A 203 mm thick asphalt wearing surface is used, but is not considered part of the structural section and is treated as additional superimposed dead load.
- The sign convention used for preliminary designs considers tension as positive and compression as negative.
- Negative deflection value indicates camber while a positive deflection means sagging.

3.4.3. Pretensioning Design

The pretensioning steel of the girder segments consists of 15 mm diameter Grade 270 low relaxation strands having an ultimate tensile strength $f_{pu} = 1860\ MPa$. The initial stress in the pretensioning strands at transfer $f_{pi} = 0.70 f_{pu} = 1302\ MPa$. The optimized design is based on the proposed optimum deflections to obtain minimum deflections using deflection balancing concept. The minimal force design is based on the general concept of prestress design of minimizing force while maximizing eccentricity. Table 3-4 presents the pretensioning design for the girder segments for unshored method of construction.

Magnel diagram is a graphical representation of the stress inequality equations. The four critical stress inequality equations are plotted for various values of the prestressing force inverse and number of prestressing strands and eccentricity values. The region which satisfies all the inequalities is termed as the feasibility domain. All the points in this region give a prestressing force and eccentricity value which satisfy all the stress limits for all the load conditions. Figure 3-4 and 3-5 represents the magnel diagrams for eccentric and harped tendon profiles for different design objectives for the Untopped case. The dashed green line represents the girder top, while the dashed red line represents the maximum eccentricity possible after meeting the minimum cover requirements. The solid blue and red lines represent the stress inequalities at the time of release of prestress and the solid yellow and gray lines represent the tension and compression stress limits at service. The final adopted values of force, corresponding number of strands and eccentricity for the pretensioning design for each case are represented by green cross marks.

3.4.3.1. Minimum Force Design

The general idea behind design of pretensioning in precast concrete members is to minimize force while maximizing eccentricity. The strands are usually placed at the bottom of the girder to achieve this objective. Generally, a design may want to minimize the number of strands in the belief that this provides the least costly solution. However, the deflections are unknown, and any hogging or sagging is built-in to the system. This result is presented in Figure 3-4. The minimum force needed to keep the stress under the specified limits is used with the maximum practical eccentricity from the magnel diagram.

Eccentric Solution

Figure 3-4(a) shows the strand layout of the girder and the magnel diagram for the eccentric tendon profile. The minimum number of strands practically possible using only eccentric tendons is found to be 38, with an effective force of 5547 kN and eccentricity of 650 mm. The minimum number of strands could not be reduced further even though the magnel diagram shows a minimum of 26 strands, because of the presence of 10 strands in the top flange of the modified precast girder.

Harped Solution

Figure 3-4(b) shows the strand layout of the girder and the magnel diagram for the harped tendon profile. The minimum number of strands practically possible using harped tendon profile is found to be 36, with an effective force of 5254 kN and eccentricity of 715 mm at center. Since only 4 out of 34 strands are harped, the end eccentricity is found to be 540 mm.

3.4.3.2. Optimized Design

In contrast to the minimum force design, it is contended that it should be possible to achieve a near level riding surface throughout (after losses) without any appreciable sagging or hogging. This solution, where the deflections are minimized is presented in Figure 3-5. The concept of deflection balancing is applied using the magnel diagram approach. The deflection control lines are shown by dashed blue lines. These lines are based on the optimum solutions given in Table 3-1.

Eccentric Solution:

Figure 3-5(a) shows the strand layout of the girder and the magnel diagram for the eccentric tendon profile. Along with the stress equations, a deflection line having $Fe = WL/9.9$ (from Table 3-1) is included into the magnel diagram to minimize the deflections. A total of 46 strands with the required effective force of 6713 kN and an eccentricity of 428 mm. The final designed $Fe = WL/9.95$ with a minimum deflection of $\pm$2.4 mm, including the long-term multipliers. The locked-in deflections are greatly reduced by implementing the deflection balancing through optimized eccentric pretensioning ($Fe = WL/9.9$, $\gamma_0 = \gamma_c$ = 0.101).

Harped Design:

Figure 3-5(b) shows the strand layout of the girder and the magnel diagram for the harped tendon profile. Along with the stress equations, deflection control line having $Fe_c = 0.121WL$ for midspan and $Fe_0 = 0.016WL$ for ends assuming the harp points as α = 0.35 (from Table 3-1) is included into the magnel diagram to minimize the deflections. A total of 38 strands with the required force of 5547 kN and an eccentricity of 625 mm and 72 mm at center and at end respectively. Out of the 38 strands, 18 strands are harped and 20 are straight. The final designed $Fe_c = 0.121WL$ and $Fe_0 = 0.014WL$ for α = 0.35 with a maximum deflection of +0.2 mm, including the long-term multipliers. The locked-in deflections are significantly reduced by implementing the deflection balancing through optimized prestress design using harped pretensioning. This aspect is elaborated upon in the following subsection.

Table 3-4: Pretensioning design for Untopped case

Profile	**Minimal force**		**Deflection balancing**	
	Eccentric	**Harped**	**Eccentric**	**Harped**
No. of strands	38	36	46	38
Initial Force, F_i (kN)	6934	6568	8391	6394
Final Force, F (kN)	5547	5254	6713	5547

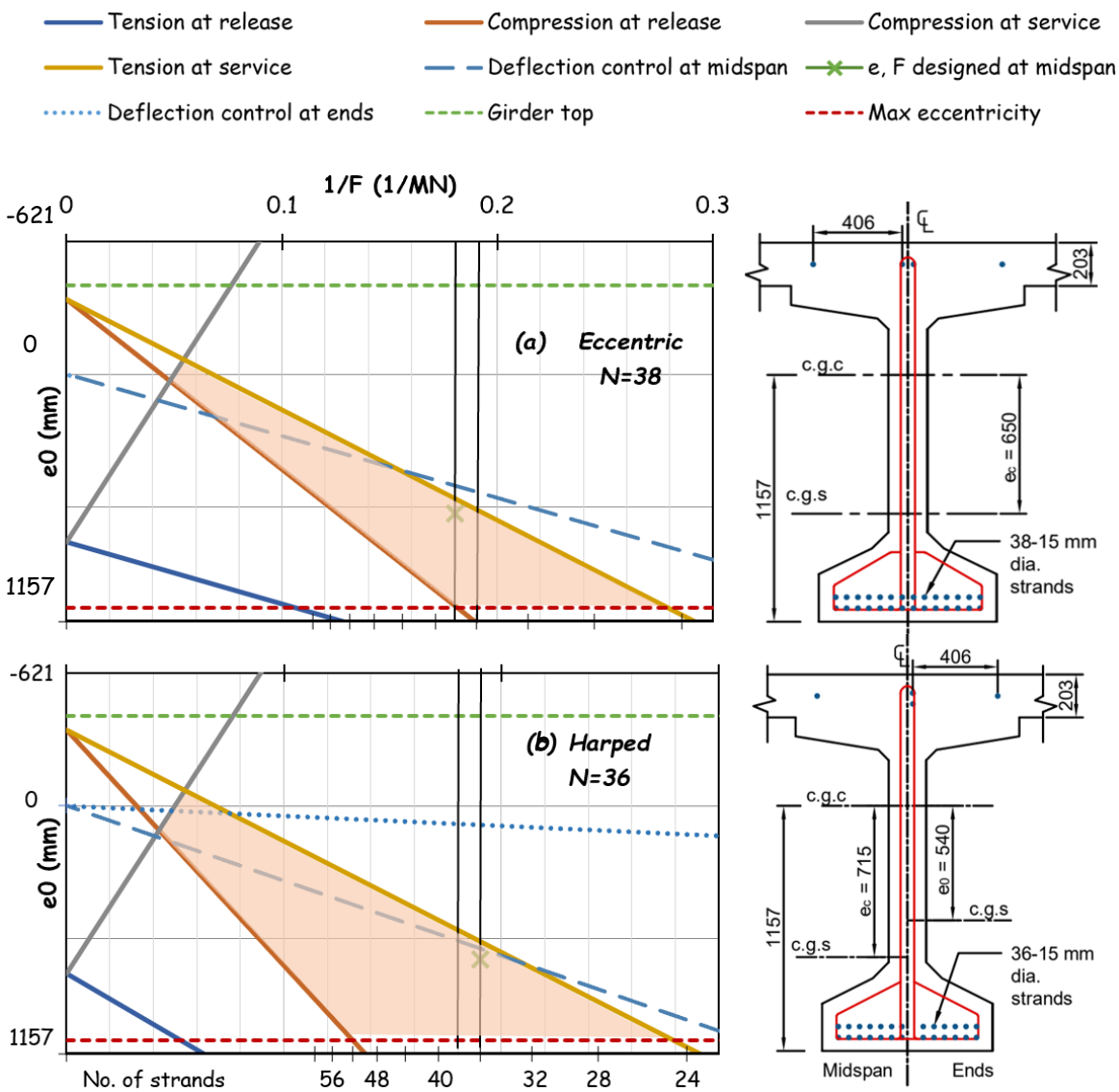

Figure 3-4: Prototype strand details for Minimal Force Prestress design for Untopped Case

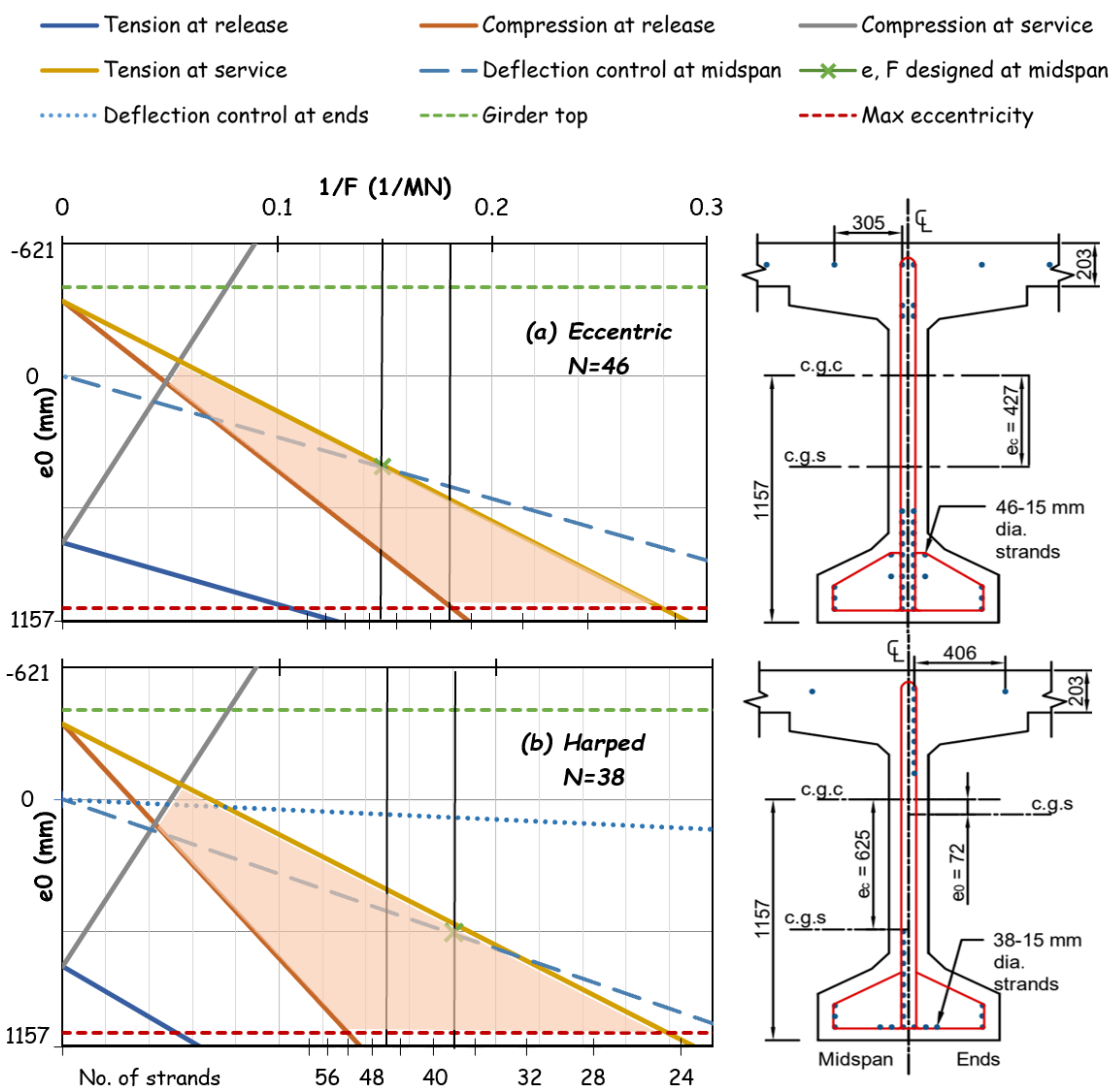

Figure 3-5: Prototype strand details for Optimized Prestress design for Untopped Case

3.4.4. Deflection Profile

Figure 3-6 and 3-7 shows the tendon profile, bending moment diagram and the deflection at various stages of construction for the eccentric tendon profile (first half portion) and for the harped tendon profile (second half portion). Figure 3-6(a) and 3-7(a) represents the tendon profiles and the adopted force and eccentricity for the two design cases. The bending moments due to the dead loads and due to the prestress force after losses are represented in Figure 3-6(b) and 3-7(b) using dashed red line and solid blue lines respectively. The resulting deflection profiles are represented in Figure 3-6(c) and 3-7(c). The deflections are various stages of construction are calculated using equations (3-3) to (3-9). A comparison between final deflection profiles for eccentric and harped tendon layouts for each design solution is presented. Dashed blue lines represent the deflection during the release of prestress. The camber of the girder increases during the period it is left in storage and the camber at erection is shown using orange solid lines. The camber of the girder sags down a little when dead load is added onto it, as seen in Figure 3-6(c) and 3-7(c) using solid green lines. Finally, the deflection under the effect of prestress force and dead load after all the long-term losses have taken place is shown using thick solid red lines. Table 3-5 presents the summary of deflections observed at each stage of construction for different prestressing solutions and tendon profiles.

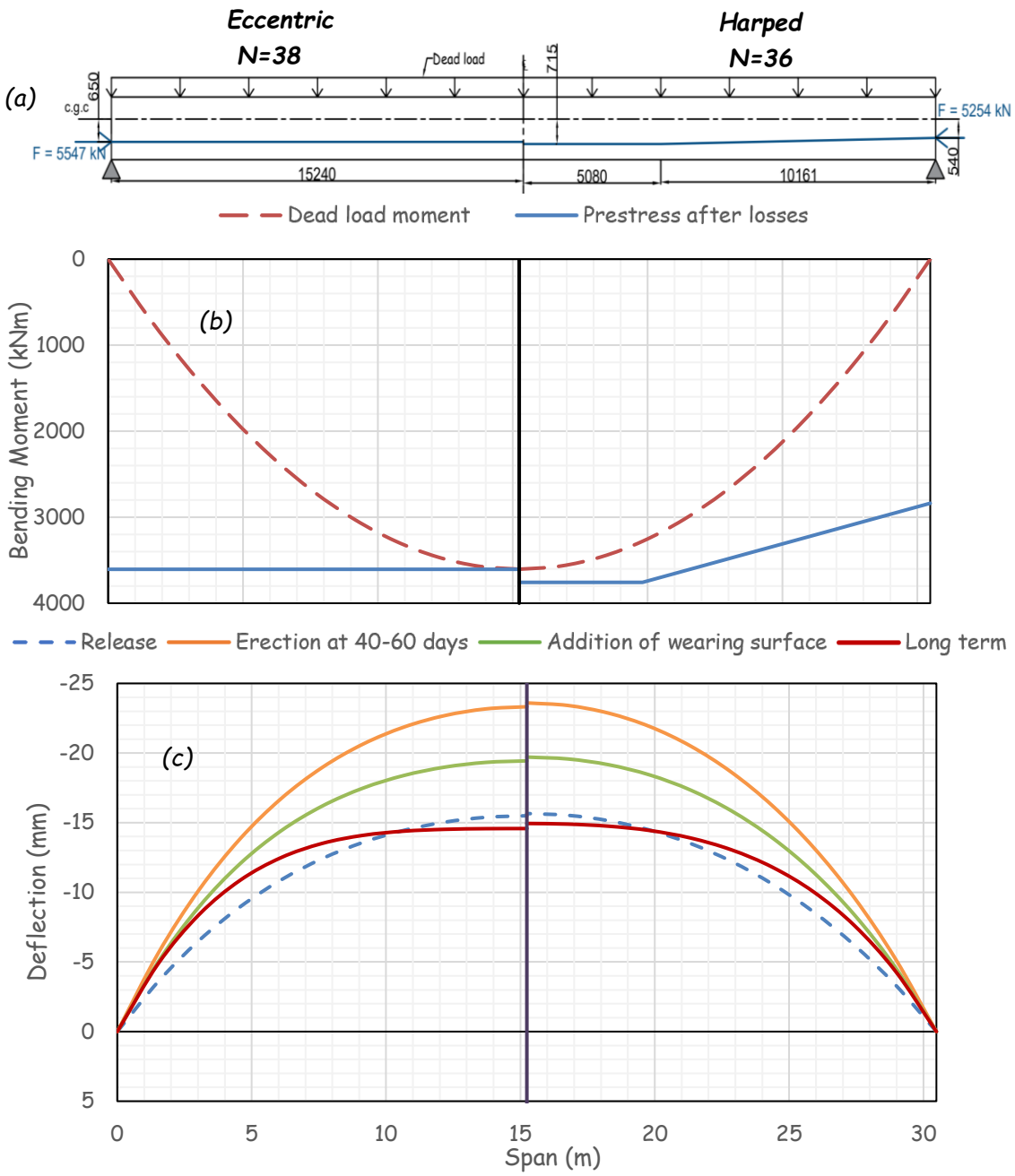

Figure 3-6: Minimal Force solutions for untopped girder using: (a) Eccentric and Harped profile; (b) resulting bending moment diagram under dead load and prestress; and (c) resulting deflection profiles under prestress and dead load

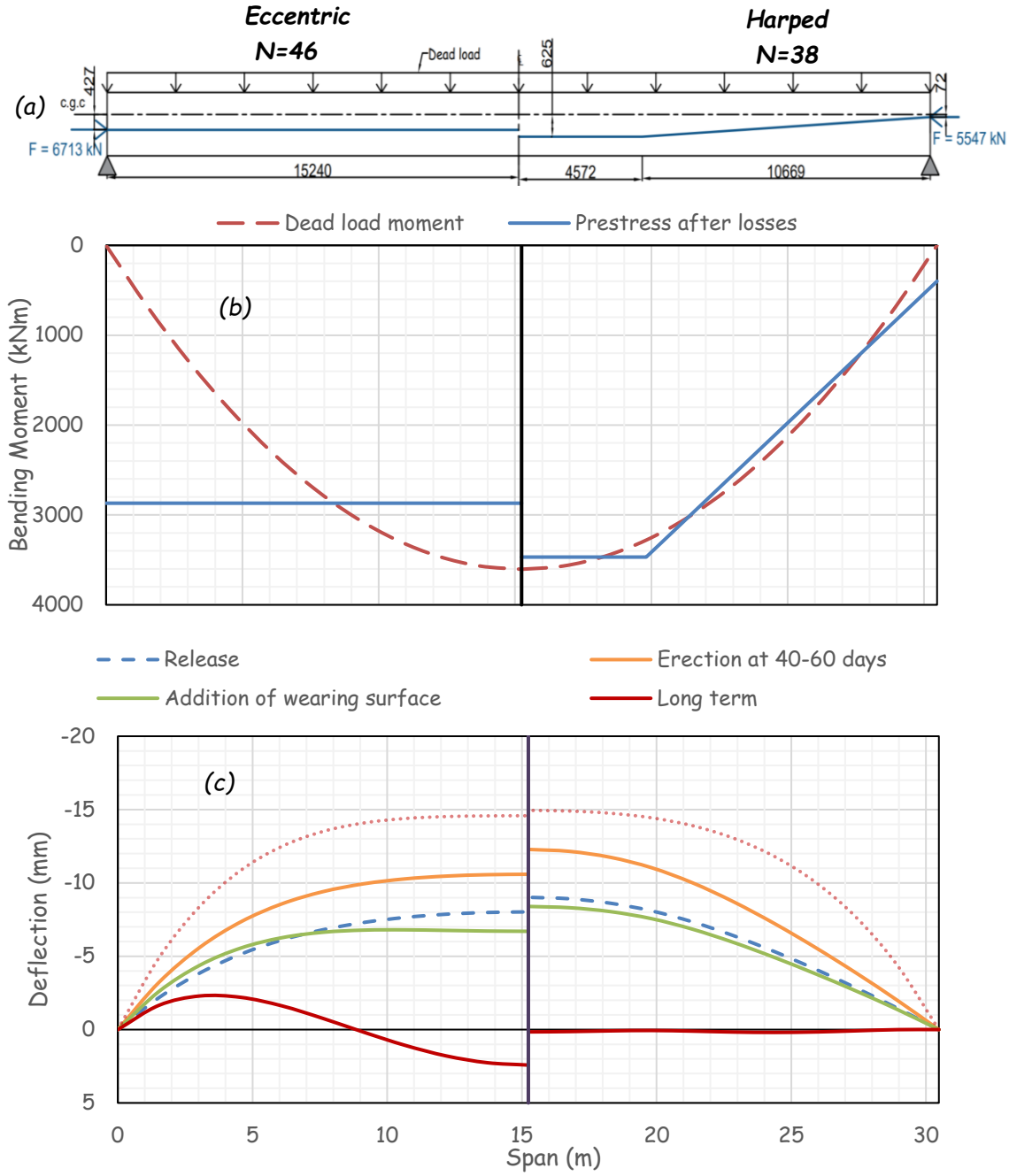

Figure 3-7: Optimized prestressing solutions for untopped girder using: (a) Eccentric and Harped profile; (b) resulting bending moment diagram under dead load; and (c) deflection profiles under combined prestress and dead load

Table 3-5: Summary of deflections for Untopped case

Solution type	No. of strands (N)	No. of harped strands	Harp point (α)	Maximum Deflections (mm)				Objective Outcome
				Release	Erection	Added dead load	Final	
Eccentric	38	-	-	-15.5	-23.3	-19.4	-14.6	Minimal strands
Harped	36	4	0.33	-15.7	-23.6	-19.7	-14.9	
Eccentric	46	-	-	-8.0	-10.6	**-6.7**	**-2.4**	Minimal deflections*
Harped	38	18	0.35	-9.0	-12.3	**-8.4**	**+0.2**	

*Indicates preferred solution outcome

3.4.5. Stress Checks

Given that stresses are more critical than the strength in prestressed concrete members, it is necessary that stresses be checked during all the construction stages to ensure a safe and durable design.

Table 3-6 and Table 3-7 summarizes the stress in the girder at ends and at midspan during all 3 stages of construction and the service limit state: (1) after pretensioning before long-term prestress losses; (2) during girder erection; (3) after the addition of superimposed dead load; (4) at service limit states. Allowable stresses are adopted from AASHTO LRFD Bridge Design Specifications (AASHTO 2017).

Figure 3-8 and 3-9 presents of variation of stress block at midspan in the girder for the optimized prestress design and for minimal force design respectively. The first row in each case shows the stresses in the section before the addition of wearing surface (superimposed dead load) and the second row represents the stress block for the section after the addition of wearing surface.

Table 3-6: Girder stresses for minimal force design at various stages for Untopped case

Stage	Section	Location	Eccentric (MPa) N = 38		Harped (MPa) N = 36		Allowable Stress Limits (MPa)	
			Midspan	Ends	Midspan	Ends		
Release	Girder	Top	-4.6	-1.0	-4.0	-1.8	-24.8	+4.1
		Bottom	-9.5	-17.3	-9.7	-14.6		
Erection	Girder	Top	-4.5	-1.0	-4.0	-1.6	-24.8	+4.1
		Bottom	-8.1	-15.9	-8.3	-13.4		
Added dead load	Girder	Top	-5.3	-1.0	-4.8	-1.6	-24.8	+4.1
		Bottom	-6.4	-15.9	-6.6	-13.4		
Long-term service	Girder	Top	-8.8	-0.9	-8.4	-1.5	-35.2	+3.8
		Bottom	+1.3	-14.6	+1.1	-12.3		

Table 3-7: Girder stresses for Optimized prestress design at various stages for Untopped case

Stage	Section	Location	Eccentric (MPa) N = 38		Harped (MPa) N = 36		Allowable Stress Limits (MPa)	
			Midspan	Ends	Midspan	Ends		
Release	Girder	Top	-6.8	-3.3	-4.8	-5.5	-24.8	+4.1
		Bottom	-8.5	-16.3	-9.1	-7.3		
Erection	Girder	Top	-6.5	-3.1	-4.7	-5.1	-24.8	+4.1
		Bottom	-7.2	-15.0	-7.8	-6.7		
Added dead load	Girder	Top	-7.3	-3.1	-5.5	-1.8	-24.8	+4.1
		Bottom	-5.5	-15.0	-6.1	-6.7		
Long-term service	Girder	Top	-10.6	-2.8	-9.0	-4.7	-35.2	+3.8
		Bottom	+2.1	-13.8	+1.5	-6.2		

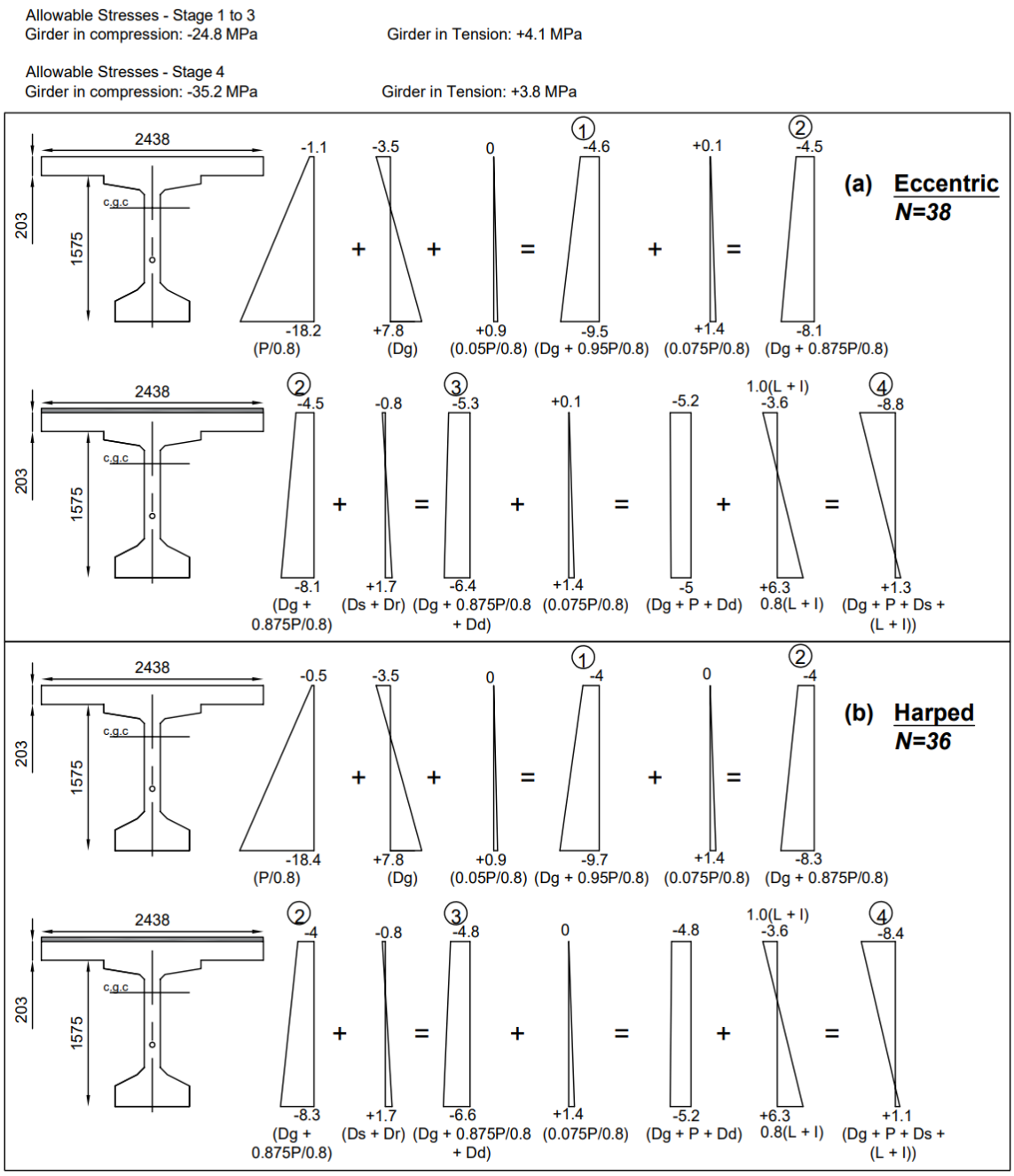

Figure 3-8: Stress at various locations for Minimal Force design (Untopped case)

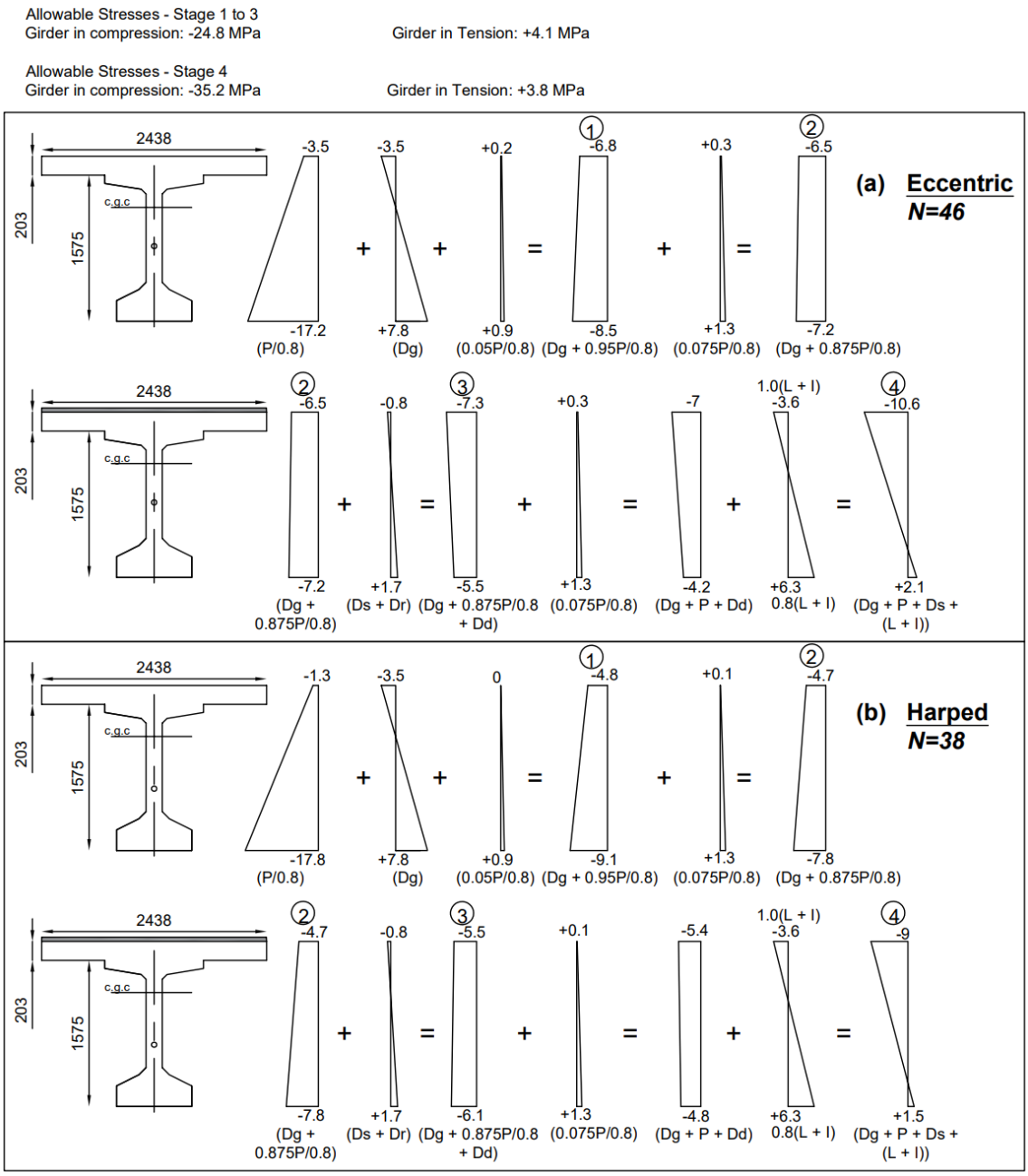

Figure 3-9: Stress at various locations for Optimized Prestressing design (Untopped case)

3.4.6. Ultimate Strength

Bending moments at ultimate limit state must be checked in order to verify that the reduced nominal flexural capacity of the girders is more than the factored ultimate flexural demand. The ultimate moment capacity of the section depends on the area of prestressing steel, force in strands, material properties of concrete and prestressing steel and the cross-section properties of the girder.

The load factors for the ultimate design moment and the reduced nominal moment strength is calculated according to AASHTO LRFD Bridge Design Specifications (AASHTO 2017). The dead load moments due to the girder self-weight and guard rails are multiplied by a factor of 1.25, the wearing surface moment is multiplied by a factor of 1.5 and the live load and impact load moments are multiplied by a factor of 1.75.

For this design, the section is tension-controlled and hence the neutral axis lies in the wide precast flange. Table 3-8 gives the results for moment demand and capacity for the bridge. The analysis shows that the capacity is greater than demand, therefore no additional reinforcement is needed.

Table 3-8: Summary of moment demand and capacity for Topped case

Capacity and Demand	Minimal Force		Deflection balancing	
	Eccentric N = 38	Harped N = 36	Eccentric N = 46	Harped N = 38
Mu, MN-m	9.9	9.9	9.9	9.9
∅Mn, MN-m	11.9	11.9	11.5	11.6
DCR	0.83	0.83	0.86	0.85

3.4.7. Shear Strength

The shear is designed according to AASHTO LRFD Specifications (AASHTO 2017). The procedure uses Modified Compression Field Theory (MCFT) to take into account the combined action of axial load, flexure and prestressing. Harped prestressing offers more resistance to shear compared to the eccentric-only profiles because of the upward reaction of the force harped strands. If the reduced nominal shear strength of the concrete is less than the factored ultimate design shear, the shear resistance can be increased by providing mild steel hoops in the section.

For this design, the shear demand on the section exceeds the reduced nominal shear capacity. Therefore, #5 double legged stirrups are provided @ 127 mm spacing for a length of 1.58 m from both ends and #5 double legged stirrups @ 305 mm spacing in the remaining portion.

3.5. Closing Remarks and findings

This chapter describes the concept of deflection balancing. This approach was introduced to minimize the deflection of the precast girder segments by pretensioning alone. Various near optimum solutions for minimum deflections using different tendon profiles were proposed. Based on the proposed design, two different application examples for a prototype bridge having eccentric and harped tendon profiles were designed for an unshored method of construction of Untopped bridge girders. The resulting deflection using the optimized prestress solutions were compared with the generally used minimal force prestress designs. Based on the results and details of each tendon profile, the following remarks and findings are drawn.

1. If post-tensioning is not applied to individual precast segments, unbalanced deflection may lead to locked-in deflections after all the long-term losses have taken place.
2. Deflection balancing technique by using pretension only solutions can effectively reduce the elastic deflections of the non-composite section and the locked-in long-term deflections of the individual precast segments for an untopped case of prestressed concrete girder construction. Deflection minimization may be done using eccentric-only prestress, harped prestress with no end eccentricity and a harped prestress solution with optimum end eccentricity.
3. Harped pretensioning is more effective than eccentric-only prestress solution in balancing the deflection of the precast segments. A harped solution with optimum end eccentricity is the most efficient pretension approach to balance the loads as well as deflection of the precast segments under self-weight.
4. For the eccentric-only solution, the minimum deflections can be obtained if the prestress moment is 0.1 times the total dead load moment.
5. For the harped prestress solutions, minimum deflections are found when the harp points lie between 0.3L to 0.5L. The theoretical minimum is found to be at 0.35L.
6. Using the deflection balancing concept for eccentric-only tendon profile reduced the long-term deflections by 84 percent with only 21 percent increase in the number of strands.

7. For a harped tendon profile, the maximum final deflection was reduced by 99 percent when the number of strands were increased by 6 percent and the concept of deflection balancing was applied.
8. These optimized prestress design approach eliminates the need for providing haunches or variable deck slab thickness during construction.

4. TOPPED PRESTRESSED CONCRETE GIRDERS

4.1. Introduction

This chapter revisits the concept of deflection balancing for prestressed concrete bridges. The long-term deflections in case of topped prestressed concrete girder bridges are more difficult to estimate, yet more critical than the untopped (non-composite) sections. In case of topped prestressed concrete girders, the hogging deflection of the precast girders is reduced somewhat after the deck is cast, but any deflections are "locked-in" once the concrete hardens. Because of the higher stiffness of the composite section compared to the non-composite section, the deck slab would not creep downwards as much as the girders. Also, when the section becomes composite at the time of erection, the rate of creep of the girder also reduces because of the higher stiffness of the composite section. This causes the bridge deck profile to remain cambered upward even after all the long-term losses have taken place and does not allow a smooth level ride for vehicles. To account for the high camber, generally the deck slabs have variable thickness or haunches during casting. This causes difficulties in the alignment of slab reinforcement and also increases the dead load on the structure, further leading to increased construction costs. Thus, the increase in moment of inertia of girders to the composite moment of inertia makes the application of deflection balancing concept to the topped prestressed concrete girder more complex.

Many studies in the past have discussed the camber variation in girders which have been cast together but are erected at different ages. O'Neil & French (2012) confirms that the girder age at erection is a source of camber variability. A difference of +-10% can be observed in the camber if the girder age at erection is 30 days or 365 days instead of the

average age of 100 days considered. It was also seen that most of the girders were shipped in the first hundred days after casting and showed much lesser camber than the design camber. It is indicated in Rosa et al (2007) that the typical age of the girders for WSDOT is 40 – 120 days before the deck slab is placed. This requires the need to consider more than one multiplier for early age erection, for most probable erection age and for mature erection age.

In this chapter, the general design philosophy for the design of topped prestressed concrete bridge is discussed. The concept of deflection balancing for the topped girders is introduced to effectively balance the long-term deflections while still satisfying the limit states. Long-term deflection multipliers for the topped case suggested by Martin (1977) are modified for the application case in consideration and the different cases of girder age at erection are compared. The final aim is to achieve as near as practicable flat deck profile after all the long-term losses have taken place. Naturally, a second objective is to minimize the prestress force.

4.2. Long-Term Multipliers

To calculate the long-term deflections for the topped (composite) section, the higher stiffness of the composite section is taken into account along with the time-dependent properties of concrete and prestressing steel. These multipliers are based on Martin's method (1977) which is also used in current practice and PCI Design Handbook (2010). The multipliers proposed by Martin (1977) are given in Table 2-1. The long-term multipliers for the downward deflection due to girder self-weight and due to slab weight differs because of the difference in the stiffness of the section after the deck slab is

hardened. The long-term multiplier for the deck is lower than the precast girder multiplier because of the higher stiffness of the composite section. Also, if the section becomes composite at the time of erection, the long-term multipliers for the precast concrete needs to be modified to account for the higher stiffness after the topping is added.

Martin (1977) makes some general assumptions in order to derive the long-term multipliers. The ratio of non-composite moment of inertia to composite moment of inertia ($I_0/\ I_c$) is assumed to be 0.65 and the age of girder erection is assumed to be 40-60 days. These assumptions do not always hold true for the modern girders. According to Tadros et al. (2011), some agencies require the girders to be at least 28 days old when the deck concrete is poured while some agencies require it to be at least 90 days old. In emergency replacement cases, girders as young as several days have been known to be installed. The cases where the girders were 6 months old have also been seen. This variation in the girder age can cause inaccurate prediction of long-term camber if a common multiplier is used for all the cases. Also, the ratio of $I_0/\ I_c$ for modern prestressed concrete girders is found to be much lower than the assumed value of 0.65. Therefore, the long-term multipliers for the precast concrete and the deck slab are derived using Martin's (1977) method for the ratio $I_0/\ I_c = 0.45$ and for 3 cases of girder erection age. The long-term deflection of the most probable case of erection at 40-60 days is minimized.

Table 4-1 represents the proposed multipliers derived using Martin's (1977) approach. The final force after all the losses is assumed to be 80 percent of initial.

Table 4-1: Modified at-erection and long-term deflection multipliers

		Composite Topping (Martin, 1977)	Modified Erection at 40-60 days (Case 1)	Modified Erection at 7 days (Case 2)	Modified Erection at 1000 days (Case 3)
	At erection:				
(1)	Deflection (downward) component – apply to the elastic deflection due to the member weight at release of prestress	1.85	1.85	1.00	2.70
(2)	Camber (upward) component – apply to the elastic camber due to prestress at the time of release of prestress	1.80	1.85	1.00	2.70
	Final:				
(3)	Deflection (downward) component – apply to deflection calculated in (1) above.	2.40	2.23	1.76	2.70
(4)	Camber (upward) component – apply to camber calculated in (2) above.	2.20	2.23	1.76	2.70
(5)	Deflection (downward) – apply to elastic deflection due to super-imposed dead load only	3.00	3.00	3.00	3.00
(6)	Deflection (downward) – apply to elastic deflection caused by the composite topping	2.30	1.89	1.89	1.89

The camber calculation at midspan using the multipliers for various stages of construction and service is given as follows:

1. Net deflection immediately after release of prestress:

$$\Delta_i = -0.95\Delta_{p,i} + \Delta_{g,i} \tag{4-1}$$

where $\Delta_{p,i}$ = deflection due to prestress only at transfer from Equation (3-4) and $\Delta_{g,i}$ = deflection due to girder self-weight at transfer from Equation (3-5).

2. Net deflection during erection at 40-60 days:

$$\Delta_e = -(F_e)\Delta_{p,i}(C_e) + \Delta_{g,i}(C_e) \tag{4-2}$$

where F_e = force at erection (0.875 for Case 1; 0.95 for Case 2 and; 0.80 for Case 3) and C_e = Multiplier for at-erection camber (From Table 4-1 (1)).

3. Net deflection immediately after the placement of deck concrete:

$$\Delta_s = -F_e\Delta_{p,i}(C_e) + \Delta_{g,i}(C_e) + \Delta_d \tag{4-3}$$

in which Δ_d = deflection due to deck weight given as:

$$\Delta_d = \frac{5}{384}\frac{W_d L^3}{E_c I_0} \tag{4-4}$$

where W_d = total weight of the deck concrete.

4. Net long-term deflection under the effect of dead load and prestress:

$$\Delta_{LT} = -(F_e)\Delta_{p,i}(C_{LT-1}) + \Delta_{g,i}(C_{LT-1}) + \Delta_d(C_{LT-2}) + (\Delta F_e)\Delta_p(C_{LT-2}) + \Delta_{sidl}(C_{LT-3}) \tag{4-5}$$

in which Δ_p = deflection due to loss in prestress after casting of deck and Δ_{sidl} = deflection due to superimposed dead load given as:

$$\Delta_p = \frac{F_i e_{02} L^2}{8E_c I_c} + \frac{F_i(e_{c2} - e_{02})L^2}{6E_c I_c}\left(\frac{3}{4} - \alpha^2\right) \tag{4-6}$$

$$\Delta_{sidl} = \frac{5}{384}\frac{W_{sidl}L^3}{E_c I_c} \tag{4-7}$$

where ΔF_e = additional loss in prestress after erection ($\Delta F_e = F_e - 0.8F_i$); C_{LT-1} = Multiplier for long-term deflection of precast concrete (From Table 4-1 (3)); C_{LT-2} = Multiplier for long-term deflection of composite deck concrete (From Table 4-1 (6)); and C_{LT-3} = Multiplier for long-term deflection of superimposed dead load on composite section (From Table 4-1 (5)).

4.3. Design Philosophy

The load balancing approach can be effectively used to create a constant state of compressive stress in the sections. However, care must be taken in the control of the deflection, given that the deck deflection multiplier is nearly half of the multiplier for the girder's self-weight, application of load balancing approach can lead to large upward camber even after all the long-term losses have taken place. The main steps of the design for unshored topped prestressed concrete bridges are outlined as follows.

4.3.1. Select the bridge cross-section

The geometry of the bridge is chosen based on the minimum stiffness required for the live load deflection according to AASHTO LRFD Bridge Design Specifications (AASHTO

2017) Article 2.5.2.6.2. Dynamic amplification factor is also multiplied to the design truck load to compute deflections.

4.3.2. Basis of Pretension Design

Determine the minimum force and number of strands required for pretensioning based on the allowable stress limits at all stages of construction and service. The minimum force is found by solving the stress inequality at the governing stage. In case of a topped prestressed concrete girder, this governing case is generally the soffit tension at service. The midspan eccentricity can be assumed as 0.4 times the girder height to get an estimate of minimum prestress force required.

Figure 4-1 represents the components of stresses which contribute to the final service stresses at the soffit and top of the girder. In the figure, $F =$ force after losses, thus the initial force at transfer with assumed 20% losses $= F_i = F/0.8$, and N$T_1 = F$ where $N =$ number of strands and $T_1 =$ force in one strand after losses.

Using the minimum force and assuming a harp point, Equation (4-5) can be equated to zero to find the relation between end eccentricity and the center eccentricity which can effectively minimize the long-term deflections.

If the long-term deflections do not ensure a nearly straight profile, change the harp point (in case of a harped tendon profile) or the force and eccentricity to try and balance the long-term deflections. The erection camber should be less than 102 mm as preferred by TxDOT. To reduce the camber, the harp points could be moved towards the center of the beam or the force/eccentricity can be reduced.

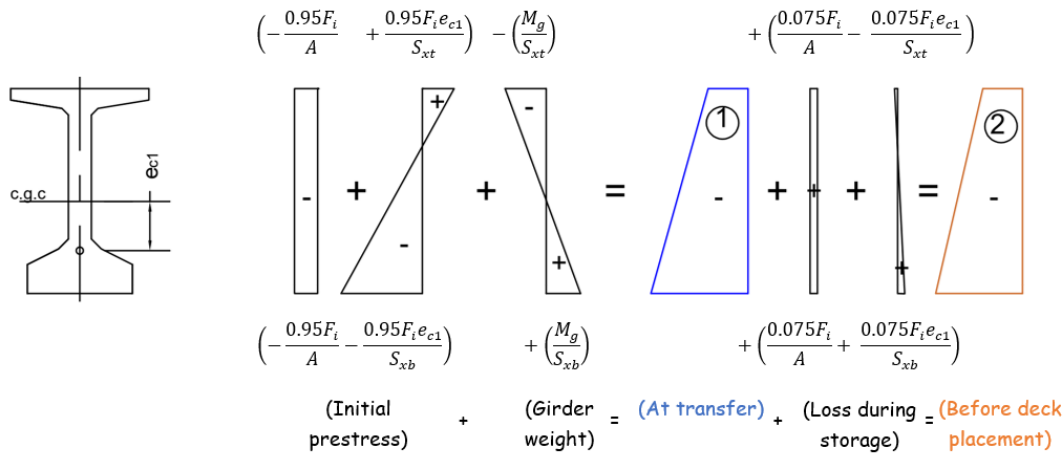

(a) Girder stress evolution up until the time of placing in the field

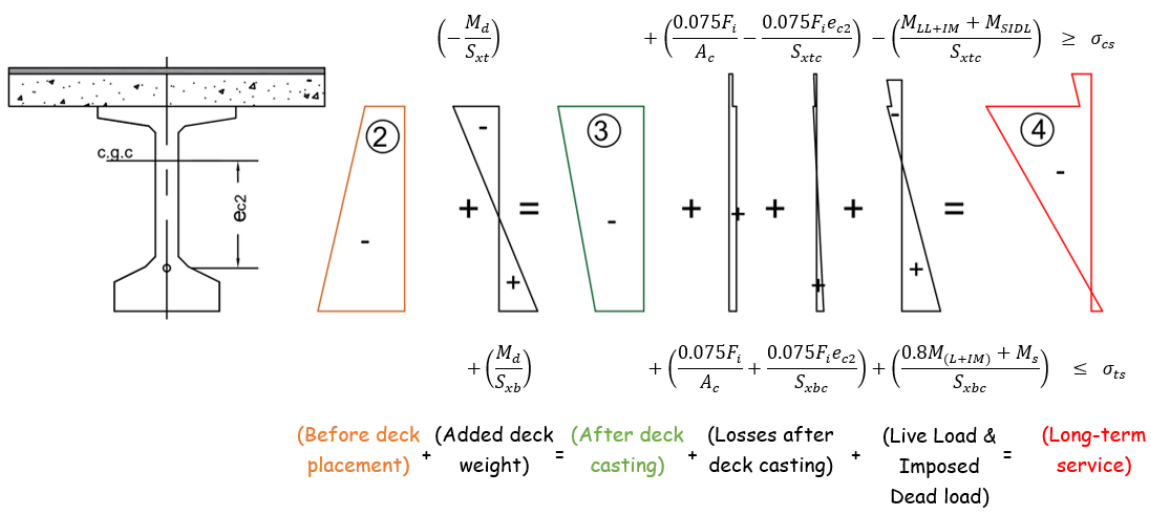

(b) From field placement, deck casting and remaining time-dependent losses for overall bridge deck plus traffic load

Figure 4-1: Stresses at the critical center span region from casting, through construction including the effects of time-dependent losses plus live load traffic effects

4.3.3. Design Verification & Checks

4.3.3.1. Stresses

Given that stresses are more critical than the strength in prestressed concrete members, it is necessary that stresses be checked during all the construction stages to ensure a safe and durable design. The stress in the girder at ends and at midspan are checked during all 3 stages of construction and the service limit state: (1) after pretensioning before long-term prestress losses; (2) during girder erection; (3) after the addition of superimposed dead load; (4) at service limit states. Allowable stresses are adopted from AASHTO LRFD Bridge Design Specifications (AASHTO 2017). Details are given in Appendix A.

4.3.3.2. Live Load Deflection

As given in Section 4.3.1, the live load deflection should be checked according to the specifications given in AASHTO LRFD Bridge Design Specifications (AASHTO 2017) Article 2.5.2.6.2. The live load deflection of the bridge considering the dynamic amplification factor should be less than L/800, where L is the span length in ft.

4.3.3.3. Ultimate Strength

Bending moments at ultimate limit state must be checked in order to verify that the reduced nominal flexural capacity of the girders is more than the factored ultimate flexural demand. The load factors for the ultimate design moment and the reduced nominal moment strength is calculated according to AASHTO LRFD Bridge Design Specifications (AASHTO 2017). If the capacity of the section is less than the ultimate design moment,

additional mild steel bars can be added in the girders or in the CIP deck to increase the capacity.

4.3.3.4. Shear Strength

The shear is designed according to AASHTO LRFD Specifications (AASHTO 2017). The procedure uses Modified Compression Field Theory (MCFT) to take into account the combined action of axial load, flexure and prestressing. Harped prestressing offers more resistance to shear compared to the eccentric-only profiles because of the upward reaction of the force harped strands. If the reduced nominal shear strength of the concrete is less than the factored ultimate design shear, the shear resistance can be increased by providing mild steel hoops in the section.

4.4. Design Case for Eccentric and Harped profile

This section demonstrates the design of topped precast prestressed concrete girder bridges using optimized prestress design. The design is based on provisions from AASHTO LRFD Bridge Design Specifications (AASHTO 2017).

4.4.1. Prototype Bridge Geometry and Girder cross-section

The geometry of the bridge is chosen based on the minimum stiffness required for the live load deflection according to AASHTO LRFD Bridge Design Specifications (AASHTO 2017) Article 2.5.2.6.2. Dynamic amplification factor of 1.33 is multiplied to the design truck load to compute deflections. Figure 4-2 shows the stiffness of the bridge based on the number of girders versus the stiffness (EI) required for different span lengths.

Figure 4-3 presents the geometry of the prototype bridge. The bridge deck cross-section is shown in Figure 4-3(a). The bridge has a total width of 14 m with a standard barrier of 0.3 m width on each side. Therefore, the total roadway width of the bridge is 13.4 m. The bridge superstructure consists of five standard Tx62 girders spaced at 3.05 m center-to-center with an overhang of 0.92 m on each side. A cast-in-place deck of thickness 216 mm and specified concrete strength of 28 MPa at service is added onto the girders as composite topping. Figure 4-3(b) shows the details of the standard Tx62 girder and Figure 4-3(c) shows the details of the composite Tx62 with 216 mm CIP slab.

Table 4-2 presents the uncracked elastic cross-section properties for the non-composite and composite for the standard and composite Tx62 girder. The live load deflection is found to be 13.7 mm compared to the allowable limit of 38 mm specified by AASHTO 2017.

4.4.2. Design Assumptions and Parameters

The prototype bridge designs are developed based on the design parameters and assumptions summarized in Table 3-3. These cross-sectional parameters and the material properties of concrete and steel were chosen based on the typical values generally adopted by TxDOT in accordance with the AASHTO LRFD Specifications (AASHTO 2017).

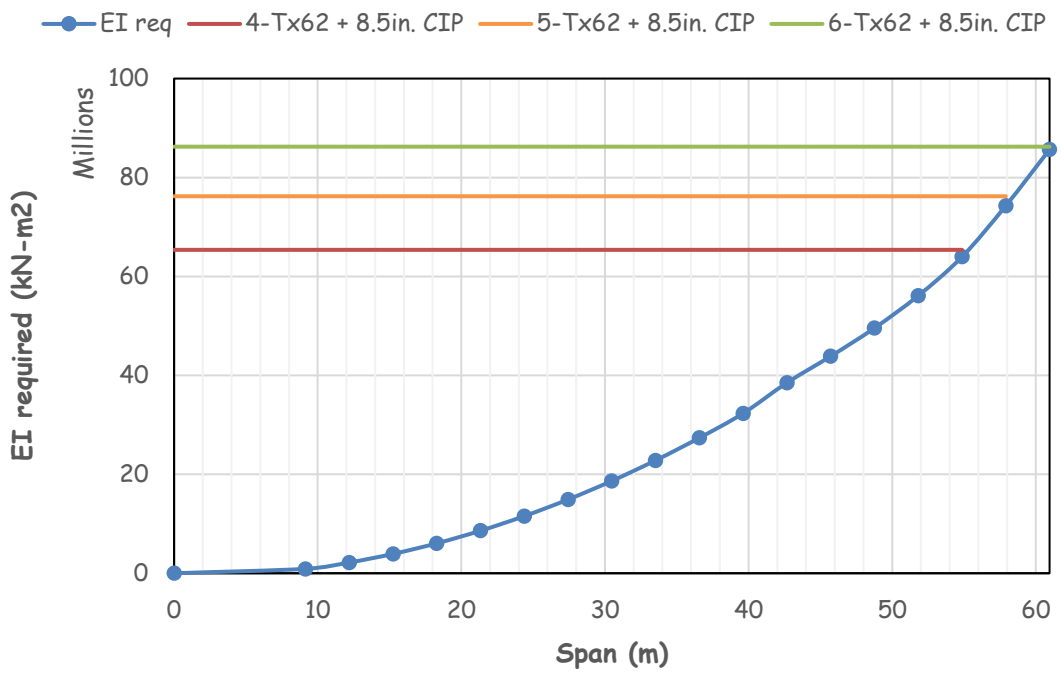

Figure 4-2: Minimum EI required for various span lengths

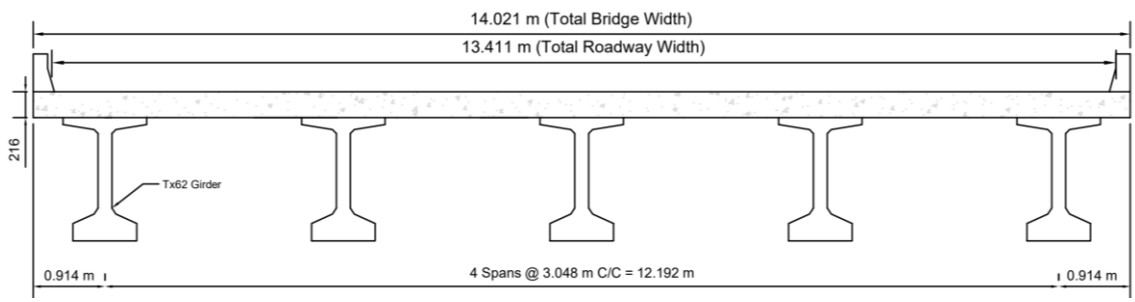

(a) Bridge deck cross-section

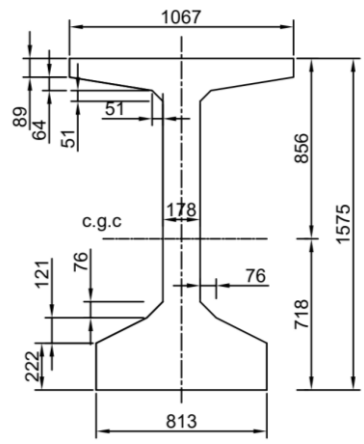

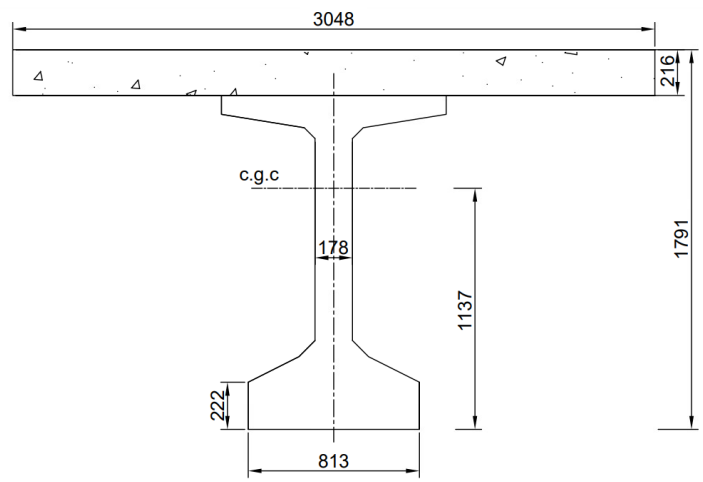

(b) Standard Tx62

$A = 0.587\ m^2$

$I_x = 0.193\ m^4$

$S_{xt} = 0.226\ m^3$

$S_{xb} = 0.269\ m^3$

(c) Composite section

$A_c = 1.038\ m^2$

$I_{xc} = 0.433\ m^4$

$S_{xtc} = 0.664\ m^3$

$S_{xbc} = 0.382\ m^3$

Figure 4-3: Prototype bridge cross-section for Untopped case

Table 4-2: Section properties for topped case

Section Property	Standard Tx62	Composite section
Total height (mm)	1575	1791
Depth of N.A. from top of girder, y_t (mm)	856	653
Depth of N.A. from girder soffit, y_b (mm)	718	1137
Area, A (m^2)	0.587	1.038
Moment of Inertia, I_x (m^4)	0.193	0.433
Section Modulus, S_{xt} (m^3)	0.226	0.664
Section Modulus, S_{xb} (m^3)	0.269	0.382

The primary designs presented in this section are developed according to the state-of-the-art and practice of girder bridges. Following are the basic assumptions which are used for these primary designs (Hueste el al., 2012).

- The construction is assumed to be done using temporary intermediate diaphragms of structural steel shapes. The negligible weight of these temporary components is not considered in the calculations.
- The entire deck slab concrete is assumed to be poured in a single operation.
- The width of the composite deck slab is transformed depending on the specified elastic modulus of the girders and the deck, respectively. The composite section properties are based on this transformed effective width.
- The sign convention used for preliminary designs considers tension as positive and compression as negative.
- Negative deflection value indicates camber while a positive deflection means sagging.

4.4.3. Pretensioning Design

The pretensioning steel of the girder segments consists of 15 mm diameter Grade 270 low relaxation strands having an ultimate tensile strength $f_{pu} = 1860\ MPa$. The initial stress in the pretensioning strands at transfer $f_{pi} = 0.70 f_{pu} = 1302\ MPa$. The optimized design is based on the deflection balancing concept to reduce the long-term deflections when the girders are 40 to 60 days old at the time of erection. Table 4-3 presents the pretensioning design for the girders for unshored method of construction.

4.4.3.1. Eccentric solution

Figure 4-4(a) shows the strand layout of the girders for the eccentric tendon profile. A total of 42 strands with the required effective force of 6130 kN and an eccentricity of 389 mm. The left half portions in Figure 4-5(a) and 4-5(b) shows the strand profile and resulting bending moments under dead load using dashed red line and effective prestress using solid blue lines for the eccentric-only tendon profile. The final designed force and eccentricity produces a minimum deflection of ± 3.8 mm, including the long-term multipliers. The locked-in deflections are greatly reduced by implementing the deflection balancing through optimized eccentric pretensioning.

4.4.3.2. Harped solution

Figure 4-4(b) shows the strand layout of the girder for the harped tendon profile. A total of 36 strands with the required force of 5254 kN and an eccentricity of 545 mm and 71 mm at center and at end respectively. Out of the 36 strands, 16 strands are harped and 20 are straight. The right half portions in Figure 4-5(a) and 4-5(b) shows the strand profile

and resulting bending moments under dead load using dashed red line and effective prestress using solid blue lines for the harped tendon profile. The final designed F, e for α = 0.35 produces a maximum deflection of -0.3 mm, including the long-term multipliers. The locked-in deflections are greatly reduced by implementing the deflection balancing through optimized prestress design using harped pretensioning.

Table 4-3: Pretensioning design for Topped case

Profile	**Deflection balancing**	
	Eccentric	**Harped**
No. of strands	42	36
Initial Force, F_i (kN)	7662	6568
Final Force, F (kN)	6130	5254

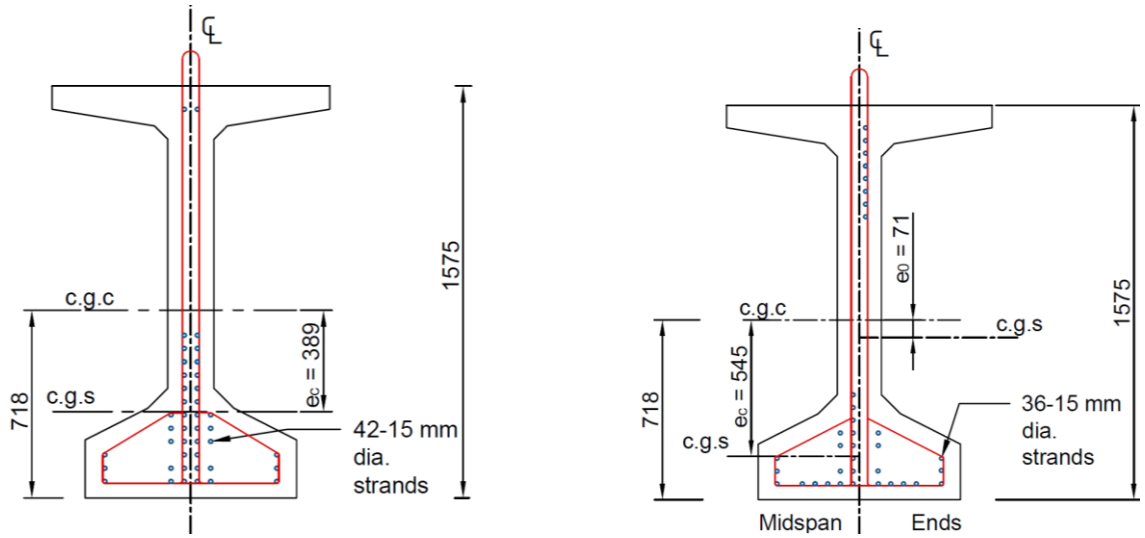

(a) Eccentric *(b) Harped*

Figure 4-4: Strand layout for Topped girders

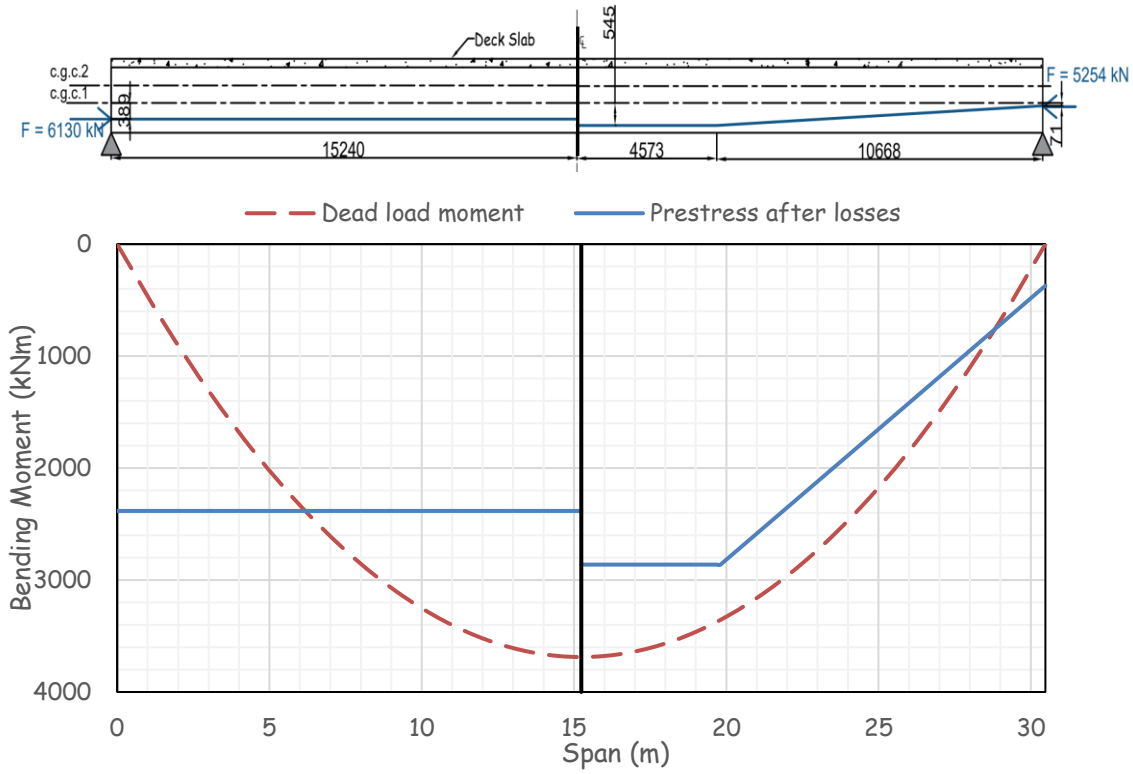

Figure 4-5: (a) Tendon layout for Topped girders and; (b) Resulting Bending Moment Diagram

4.4.4. Deflection Profile

Figure 4-6 shows the tendon profile with the adopted force and eccentricities, and the deflection at various stages of construction for the eccentric tendon profile (first half portion) and for the harped tendon profile (second half portion). The resulting deflection profiles are represented in Figure 4-6(a), 4-6(b) and 4-6(c) for different ages of girder erection. The deflections are various stages of construction are calculated using equations (4-1) to (4-5). A comparison between final deflection profiles for eccentric and harped tendon layouts is presented. Dashed blue lines represent the deflection during the release of prestress. The camber of the girder increases during the period it is left in storage and the camber at erection is shown using orange solid lines. The camber of the girder sags down a little when dead load is added onto it, as seen in Figure 4-5 using solid green lines. Finally, the deflection under the effect of prestress force and dead load after all the long-term losses have taken place is shown using solid red lines.

Figure 4-6(a) provides the deflections for the most probable case when girders are 6 to 8 weeks old during erection; Figure 4-6(b) represents the case when the girders are erected at early age (7 days) and; Figure 4-6(c) represents the case when the girders are erected after 1000 days (mature age). Since the third case (mature age) indicate that the girders are kept in storage for a long time, all the long-term losses have already taken place and the deflections are locked-in. The second case indicates that the girders are loaded before the concrete has matured and hence show higher downward deflections. Table 3-5 presents the summary of deflections observed at each stage of construction for different prestressing solutions and tendon profiles.

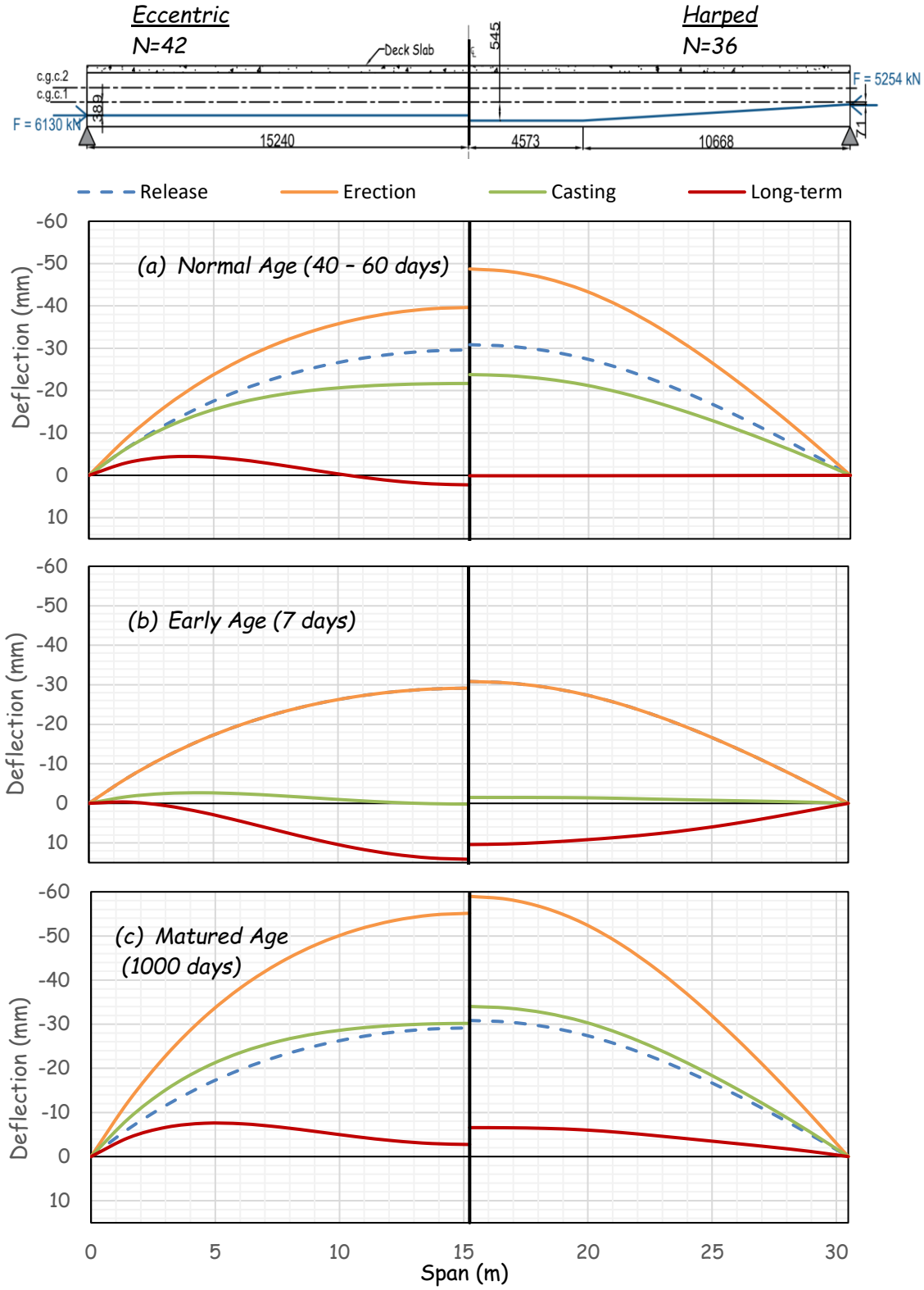

Figure 4-6: Resulting deflection profiles under prestress and dead load for optimized prestress design of topped girders

Table 4-4: Summary of deflections for Topped case

Stage/ Cases	Eccentric (mm) N = 42			Harped (mm) N = 36		
	Normal	Early Age	Mature Age	Normal	Early Age	Mature Age
Release	-29.2	-29.2	-29.2	-30.8	-30.8	-30.8
Erection	-39.0	-29.2	-55.1	-49.7	-30.8	-58.3
Casting	-20.9	-2.7	-30.2	-23.5	-1.5	-33.7
Long-term	±3.8	+14.2	-7.6	-0.3	-10.3	-6.5

4.4.5. Stress Checks

In case of prestressed concrete design, the stresses are more critical than the strength. Thus, it is necessary that stresses be checked during all the construction stages to ensure a safe and durable design.

Table 4-5 summarizes the stress in the girder for the most probable normal age case. The stresses are checked during all 3 stages of construction and the service limit state: (1) after pretensioning before long-term prestress losses; (2) during girder erection; (3) after the addition of superimposed dead load; (4) at service limit states. Allowable stresses are adopted from AASHTO LRFD Bridge Design Specifications (AASHTO 2017). The compressive stresses are checked for Service I limit state and Service III stresses are considered for the tensile stresses at service.

Figure 4-7 and 4-8 presents of variation of stress block at midspan in the girder for the eccentric and harped optimized prestress design respectively. The first row in each case shows the stresses in the section before the casting of the deck (non-composite section

stage 1 and 2) and the second row represents the stress blocks for the loads and forces acting on the composite section (stage 3 and 4).

Table 4-5: Girder stresses for optimized prestressing design at various stages for Topped case

Stage	**Section**	**Location**	**Eccentric (MPa) N = 42**		**Harped (MPa) N = 36**		**Allowable Stress Limits (MPa)**	
			Midspan	End	Midspan	End		
Release	Girder	Top	-6.9	+0.2	-2.6	-8.7	-24.8	+4.1
		Bottom	-16.9	-22.9	-17.3	-12.3		
Erection	Girder	Top	-6.9	+0.2	-2.9	-8.0	-24.8	+4.1
		Bottom	-15.1	-21.1	-15.5	-11.3		
Deck Casting	Girder	Top	-14.9	+0.2	-10.9	-8.0	-24.8	+4.1
		Bottom	-8.4	-21.1	-8.8	-11.3		
Long-term service	Girder	Top	-18.3	+0.1	-14.2	-7.3	-35.2	+3.8
		Bottom	+1.9	-20.3	+1.4	-10.4		
	Deck	Top	-3.4	-0.1	-3.5	+0.2	-16.6	+0.4
		Bottom	-2.2	+0.1	-2.2	+0.2		

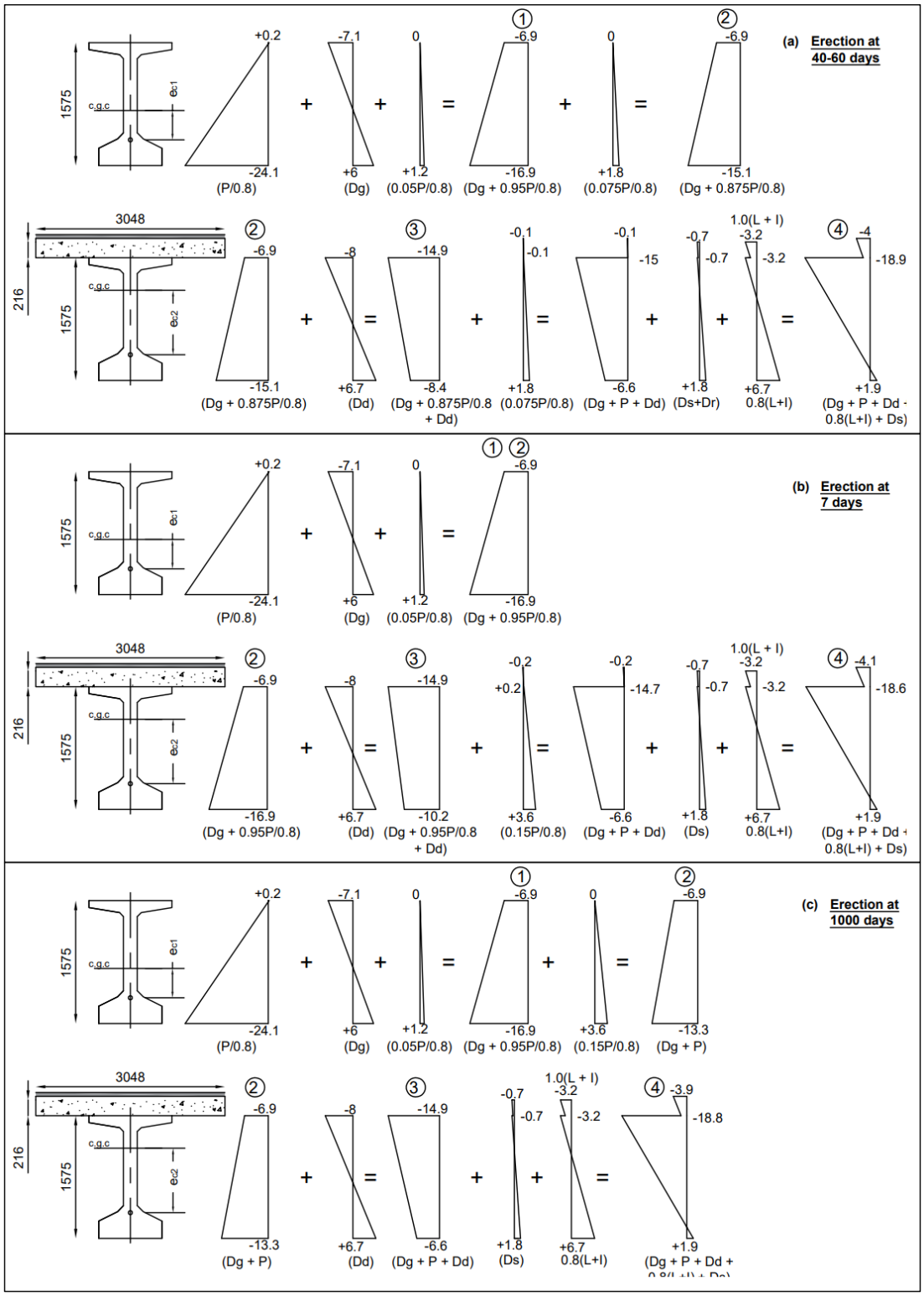

Figure 4-7: Stress at various locations for Optimized Eccentric Prestress design for Topped case

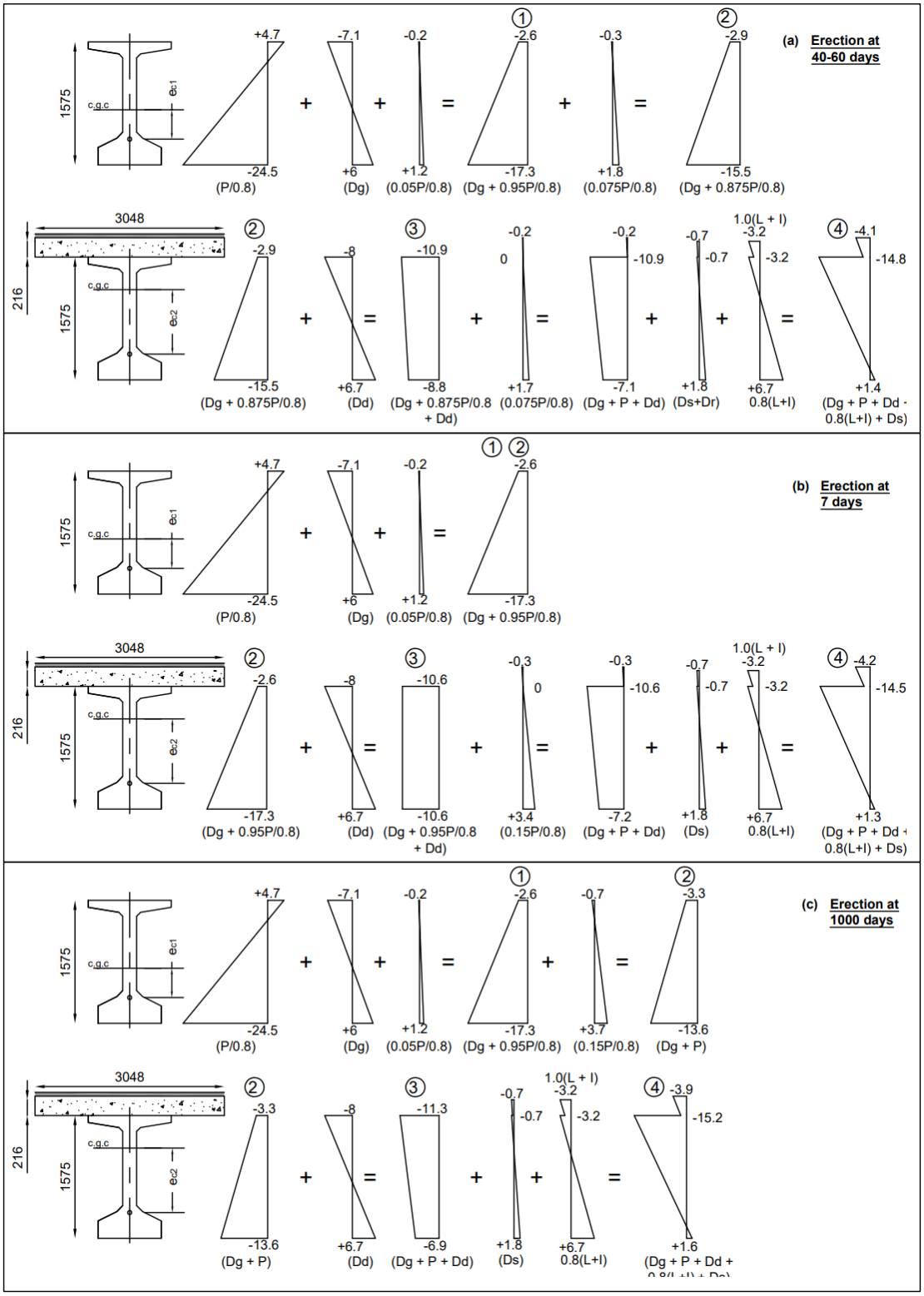

Figure 4-8: Stress at various locations for Optimized Harped Prestress design for Topped case

4.4.6. Ultimate Strength

The moment strength should be checked at ultimate load conditions to ensure ultimate load conditions. The nominal reduced flexural capacity of the bridge section should be higher than the factored ultimate flexure demand on the section. The ultimate moment capacity of the section depends on the area of prestressing steel, force in strands, material properties of concrete and prestressing steel and the cross-section properties of the girder. The dead load moments due to the girder self-weight, deck weight and guard rails are multiplied by a factor of 1.25, the wearing surface moment is multiplied by a factor of 1.5 and the live load and impact load moments are multiplied by a factor of 1.75 as specified in AASHTO LRFD Bridge Design Specifications.

For this design, the section is tension-controlled and hence the neutral axis lies in the CIP slab. The deck reinforcement consists of #4 bars @ 229 mm o.c. spacing provided at the top and bottom in both transverse and longitudinal directions. This deck reinforcement is representative of the typical reinforcement provided for concrete bridges by TxDOT; specified by (TxDOT, January 2020). Table 4-6 provides the moment demand and capacity for the bridge. The capacity is found to be greater than demand.

Table 4-6: Summary of moment demand and capacity for Topped case

Capacity and Demand	Eccentric N = 42	Harped N = 36
Mu (MN-m)	10.6	10.6
ØMn (MN-m)	14.6	14.1
DCR	0.73	0.75

4.4.7. Shear Strength

The reduced nominal shear capacity is calculated according to AASHTO LRFD Bridge Design Specification (AASHTO 2017). The combined effect of concrete strength and the reaction force because of prestressing is considered in the calculations.

For this design, the shear demand on the section exceeds the reduced nominal shear capacity. Therefore, #5 double legged stirrups are provided @ 127 mm spacing for a length of 1.58 m from both ends and #5 double legged stirrups @ 305 mm spacing in the remaining portion.

4.5. Closing Remarks and Findings

This chapter extends the concept of deflection balancing to topped prestressed concrete girders. A design approach to minimize the deflection of the topped precast girder segments by pretensioning alone was developed. Based on this proposed design approach, application examples for a prototype bridge having eccentric and harped tendon profiles were designed for an unshored method of construction of topped bridge girders. The resulting deflections using optimized prestressing design were discussed assuming the girders were 40 to 60 days old at the time of erection. The change in deflections were observed when the ages of girders at the time of erection were varied. Based on the results and details of each tendon profile, the following remarks and conclusions are drawn.

1. Topped girders (composite sections) may have higher locked-in deflections than the untopped girders (non-composite) if not properly dealt with during the design.
2. These optimized prestress design approach may permit elimination of variable depth haunches or variable deck slab thickness during construction.

3. Deflection balancing may effectively reduce the locked-in long-term deflections of the individual precast segments for topped case of prestressed concrete girder construction. Deflection minimization may be achieved using either eccentric-only prestress, harped prestress with no end eccentricity, or a harped prestress solution with optimum end eccentricity.
4. Harped pretensioning is more effective than the eccentric-only prestress solution in balancing the deflection of the precast segments. A harped solution with optimum end eccentricity is the most efficient pretension approach to balance the loads as well as deflection of the precast segments under self-weight.
5. Using the deflection balancing concept for eccentric-only tendon profile, it was observed that the long-term deflections may be as low as 4 mm for normal age girders.
6. For a harped tendon profile, the maximum final deflection was found to be as low as 0.3 mm when the girders are 6 to 8 weeks old at the time of erection.
7. If the age of the girder varies from the normal age (~6 weeks) and is not considered in the design, the deflections for mature age girders do not deviate much from the normal age. But, in case of early age of girders during erection, variable slab thickness or haunch may be needed because of lower strength (and stiffness) of concrete during early loading.
8. The difference in final stresses for different cases of girder erection is negligible, but the stresses at the time of erection and deck casting differ appreciably when the age of girders is different.

5. SUMMARY, CONCLUSIONS AND RECOMMENDATIONS

5.1. Summary

This thesis reviewed the various models and research available to accurately predict the long-term deflections of a prestressed concrete bridge girder and proposed systematic solutions to minimize the final long-term deflections under dead load and effective prestress. The first chapter provided an introduction of the project and the motivation behind this thesis. The second chapter provided a review of literature of the factors affecting the long-term camber and deflection of prestressed concrete members. Existing models and methods for the prediction of these deflections are reviewed. The third chapter introduced and used the concept of deflection balancing for the untopped bridge girder for an eccentric and harped tendon profile. This included developing optimum relations between harp point, effective force and strand eccentricity. Bridge design examples using minimal force and using proposed optimized prestress design were presented and compared. The fourth chapter expanded the concept of deflection balancing to topped bridge girders for unshored method of construction. The basis of design and design philosophy incorporating deflection balancing is discussed. The long-term multipliers for creep and shrinkage are modified to match modern girder properties. Lastly, the deflections and stresses for different ages of girder at erection were compared.

5.2. Key findings and conclusions

The following conclusions may be drawn from this research project:

If pretensioning is applied to individual girder segments instead of parabolic draped post-tensioned tendons, it may lead to unbalanced deflections because of locked-in deflections after all the losses have taken place. For this reason, a deflection balancing technique needs to be applied for pretension only solutions to effectively reduce the locked-in long-term deflections of the prestressed concrete girders. Deflection minimization may be done using eccentric-only prestress, harped prestress with no end eccentricity and a harped prestress solution with optimum end eccentricity. Harped pretensioning is more effective than an eccentric-only prestress solution in balancing the deflection of the precast segments. A harped solution with optimum end eccentricity is the most efficient pretension approach to balance the loads as well as minimize deflections of the precast segments under self-weight.

The proposed normalized deflection control equations for effective force, harp point and eccentricity can significantly reduce: (a) the long-term deflections for the untopped girders and; (b) the elastic at-erection camber for all cases. For the untopped case using an eccentric-only solution, the minimum deflections may be obtained if the prestress moment is 0.1 times the total dead load moment. While for a harped case, minimum deflections are found when the harp points lie between 0.3L to 0.5L. The theoretical minimum is found to be at 0.35L. Using the deflection balancing concept for an untopped case with an eccentric-only tendon profile reduced the long-term deflections by 84 percent with only 22 percent increase in the number of strands. Optimized harped prestress equation can

reduce the final deflection by 99 percent when the number of strands were increased by only 6 percent when the concept of deflection balancing was applied. Such optimized prestress design approaches eliminate the need for providing haunches or variable deck slab thickness during construction.

Topped girders (composite sections) may have higher locked-in deflections than the untopped girders (non-composite) if not properly dealt with, by design. Using the deflection balancing concept for the eccentric-only tendon profile, it was observed that the long-term deflections may be as low as 3.8 mm for normal age girders. For a harped tendon profile, the maximum final deflection was found to be as low as 0.3 mm when the girders were 6 to 8 weeks old at the time of erection. If the age of the girder varies from the normal age and is not considered by design, the deflections for mature age girders do not deviate much from the normal age. But, in case of early age of girders during erection, variable slab thickness or haunch may be needed because of a lower strength (less stiff) concrete during loading. The difference in final stresses for different cases of girder erection is negligible, but the stresses at the time of erection and deck casting differ appreciably when the age of the girders is different.

5.3. Answering the Research Questions

Based on the introduction presented in Chapter 1, three research questions were posed. In what follows, the questions are restated, and answers presented.

Question 1: *If the prestress is to remain straight and eccentric, how can the force and eccentricity be optimized for both topped and un-topped cases, to obtain the desirable flat-as-possible outcome after losses?*

To effectively balance the deflections in case of an untopped case, the proposed relation between the force and eccentricity $Fe = WL/9.9$ should be adopted. The application examples show that the resulting final long-term deflection was reduced by 84 percent with an increase of 21 percent in the number of strands when the prestress design was optimized using the optimum relations in contrast to the deflections obtained using minimal force design.

In case of a topped prestress girder, the complexity increases because of the composite effect of the section at service. The ratio of non-composite to composite moment of inertia varies from section to section and the higher stiffness of composite section causes the deck to deflect less than the girder. In the particular design example presented, the long-term deflections are minimized using a straight tendon when $Fe = WL/12.3$. The maximum final deflection observed is 3.8 mm.

Question 2: *If a harped solution is possible, what should be the harping distance and central and end eccentricities for the girder for topped and un-topped cases and how can this be made up (in practical terms) in terms of the number of straight v/s harped tendons?*

To effectively balance the deflections in case of an untopped case, the normalized deflection profiles indicate that the theoretical minimum deflection is obtained when the harp points are at 0.349L from each support. The recommended values of harp points are 0.3L and 0.33L for a purely harped solution with no end eccentricity and 0.35L and 0.33L

for a harped solution with optimum end eccentricity. The proposed relation between the force, eccentricities and the harp points are tabulated in Table 3-1. The application examples show that the resulting final long-term deflection was reduced by 99 percent with the increase of 6 percent in number of strands when the prestress design was optimized using the optimum relations in contrast to the deflections obtained using minimal force design.

In case of a topped prestress girder, the complexity increases because of the composite effect of the section at service. The ratio of non-composite to composite moment of inertia varies from section to section and the higher stiffness of composite section causes the deck to deflect lesser than the girder. In the particular design example presented, the long-term deflections are minimized using a harped tendon profile anchored at 0.35L when $Fe_c = WL/10.2$. The maximum final deflection observed is 0.3 mm.

Question 3: *For the topped case, what is the effect of variation in the age of girder at erection considering eccentric and harped tendon profiles on the long-term deformation of the bridge?*

If the age of the girder varies from the normal age (about 6 weeks) and is not considered in the design, the deflections for mature age girders do not deviate much from the normal age. But, in case of early age of girders during erection, variable slab thickness or haunch may be needed because of lower strength of concrete during loading.

The deflections observed for girders erected at 7 days was observed to be +14 mm (eccentric) and +10 mm (harped); the deflections for girders erected at 1000 days was observed to be -8 mm (eccentric) and -6 mm (harped) of the ideal $\pm$4 mm (eccentric) and

±0.3 mm (harped) for the average 6 to 8 weeks old girders. This shows that the girders erected at 1000 days are within construction tolerances and would not have any significant effect on the ride quality. But, when the girders are erected at 7 days, the concrete strength at the time of loading is less than the specified design strength leading to significant sagging of the girders after the long-term losses have taken place.

5.4. Limitations of the work

Caveats on this work and what can be done about them include:

1. The long-term multipliers used herein are, in essence, universal averages. It is expected that local or regional variations will exist but not be markedly different. Nevertheless, during fabrication and casting the girders, the design assumptions should be revisited and the prestress layout adjusted, if necessary to be based on regional loss calculations.
2. In situ deflections for topped girders depend on the ratio of the precast and in situ concrete strengths. Herein this is assumed to be 60 MPa (girder) and 28 MPa (deck). The deflections will be marginally different for different ratios. Therefore, an assessment should be made based on the expected in situ strengths. Again, this may mean the layout should be adjusted accordingly.

5.5. Future Research

Based on the research, the following is the scope of future work.

In case of long-span bridge construction, simply supported bridges do not seem like a feasible choice because of the high moments at mid-span. Also, because of the

restrictions on length and weight during transportation and handling, need arises for the bridge sections to be made continuous. The continuity in such bridges is provided using a combination of pretensioning and post-tensioning applied at various stages of construction. For this reason, the deflection balancing concept for continuous prestressed concrete bridges needs to be developed. The net deflections due to the effect of prestressing and moments at each support and midspan should be considered.

The time dependent properties of concrete and prestressing steel have a significant effect on the stresses and the deflections at each stage. A conservative value of the creep and shrinkage parameters or overprediction of prestress losses will lead to overestimated camber measurement and lead to hogging deflections while an underestimated value of these parameters may lead to excessive sagging over time and can also cause cracking. Hence detailed calculations or experimental study needs to be conducted in order to accurately determine appropriate regional or precasting plant-specific long-term deflection multipliers.

REFERENCES

ACI Committee 209. (1992). *Prediction of Creep, Shrinakge, and Temperature Effects in Concrete Structures (ACI 209R-92).* Farmington Hills, MI: American Concrete Institute.

American Association of State Highway and Transportation Officials (AASHTO). (2017). *AASHTO LRFD Bridge Design Specifications* (8th ed.). Washington, DC.

Baie, R. (2017). *In-Span Splicing for Continuous Prestressed Concrete Girder Bridges.* PhD Dissertation, Texas A&M University, Zachry Deparment of Civil Engineering.

Bazant, Z. P., & Baweja, S. (2000). Creep and Shrinkage Prediction Model for Analysis and Design of Concrete Structures: Model B3. *The Adam Neville Symposium: Creep and Shrinkage - Structural Design Effects, SP-194*, 1-83.

fib. (2010). *fib Model Code for Concrete Structures.* Wilhelm Ernst & Schm.

Gardner, N. J., & Lockman, M. J. (2001, March-April). Design Provisions for Drying Shrinkage and Creep of Normal-Strength Concrete. *ACI Materials Journal, 98*(2), 159-167.

Ghali, A., Favre, R., & Elbadry, M. (2002). *Concrete Structures - Stresses and Deformation* (Third ed.). London: Spon Press.

Gilbertson, C. G., & Ahlborn, T. M. (2004, Dec 6). A Probabilistic Comparison of Prestress Loss Methods in Prestressed Concrete Beams. *PCI Journal, 49*(5), 52-69.

Hinkle, S. D. (2006). *Investigation of Time-Dependent Deflection in Long-span, High-strength, Prestressed Concrete Bridge Beams.* Master of Science, Thesis, Virginia Polytechnic Institute and State University, Blacksburg.

Honarvar, E., Nervig, J., He, W., Sritharan, S., & Matt Rouse, J. (2015). *Improving the Accuracy of Camber Predictions for Precast Prestensioned Concrete Beams.* Final Report Appendices, Iowa State University, Bridge Engineering Center, Ames.

Hueste, M. B., Mander, J. B., & Parkar, A. S. (2012). *Continuous Prestressed Concrete Girder Bridges Volume 1: Literature Review and Preliminary Designs.* Texas Department of Transportation.

Jayaseelan, H., & Russell, B. W. (2007). *Prestress Losses and the Estimation of Long-term Deflections and Camber for Prestressed Concrete Bridges.* Final Report, Oklahoma State University, School of Civil Environmental Engineering.

Kamatchi, P., Rao, K. B., Dhayalini, B., Saibabu, S., Parivallal, S., Ravishankar, K., & Iyer, N. R. (2014, Nov/Dec). Long-Term Prestress Loss and Camber of Box-Girder Bridge. *ACI Sturctural Journal, 111*(6), 1297-1306.

Lee, J.-H., Lim, K.-M., & Park, C.-G. (2018). Modified PCI Multipliers for Time-Dependent Deformation of PSC Bridges. *Advances in Civil Engineering*.

Lin, T. Y., & Burns, N. H. (1981). *Design of Prestressed Concrete Structures.* Hoboken, NJ: John Wiley & Sons, Incorporated.

Mante, D. M., Barnes, R. W., Isbiliroglu, L., Hofrichter, A., & Schindler, A. K. (2019). Effective Strategies for Improving Camber Predictions in Precast, Prestressed

Concrete Bridge Girders. *Journal of Transportation Research Record, 2673*(3), 342-354.

Martin, L. D. (1977, January-February). A Rational Method for Estimating Camber and Deflection of Precast Prestressed Members. *PCI Journal*.

Naaman, A. E. (2004). *Prestressed Concrete Analysis and Design: Fundamentals* (2nd ed.). (I. Naaman, Ed.) Ann Arbor, Michigan, USA: Techno Press 3000.

O'Neill, C. R., & French, C. E. (2012). *Validation of Prestressed Concrete I-Beam Deflection and Camber Estimates.* University of Minnesota, Department of Civil Engineering. St. Paul: Minnesota Department of Transportation, Research Services.

Parchure, A. (August 2013). *Design of Continuous Prestressed Concrete Spliced Girder Bridges.* Master of Science Thesis, Texas A&M University, Zachry Department of Civil Engineering, College Station.

PCI Design Handbook (7th ed.). (2010). Precast/Prestressed Concrete Institute.

Rizkalla, S., Zia, P., & Storm, T. (2011). *Predicting Camber, Deflection, and Prestress Losses of Prestressed Concrete Members.* Final Report, North Carolina State University, Constructed Facilities Laboratory, Raleigh.

Rosa, M. A., Stanton, J. F., & Eberhard, M. O. (2007). *Improving Prediction for Camber in Precast, Prestressed Concrete Bridge Girders.* Final Research Report, University of Washington, Washington State Transportation Center (TRAC).

Sarremejane, T. M. (2014). *Analysis of Short and Long Term Deformations in a Continuous Precast Prestressed Concrete Girder*. Master of Science Thesis, Texas A&M University, Zachry Department of Civil Engineering, College Station.

Shams, M., & Kahn, L. F. (2000). *Time-Dependent Behavior of High-Performance Concrete Bridge.* Georgia Tech , Structural Engineering. Georgia Department of Transportation Research.

Tadros, M. K., Fawzy, F., & Hanna, K. E. (2011, December). Precast, prestressed girder camber variability. *PCI Journal, 56*(1), 135-154.

TxDOT. (January 2020). *TxDOT Bridge Design Manual - LRFD.* Bridge Divison. Austin, Texas: Texas Department of Transportation.

APPENDIX A

DESIGN SPECIFICATION DETAILS USED IN THIS RESEARCH

A.1 OVERVIEW

The load balancing approach for a prestressed concrete bridge uses post-tensioned (PT) draped parabolic tendons to effectively balance all the dead load moments and deflections. But generally, pretensioning is preferred for precast portions of a prestressed concrete bridge. Use of harped pretensioned tendon profile may balance the dead load moment but leaves residual end moments. The end moments may cause the girder segments to hog up and these become locked-in when the deck is cast. Therefore, in order to reduce the construction delays and costs and increase rider comfort, the aim is to achieve a nearly flat deck profile after all the prestress losses have taken place.

Two different approaches commonly used for prestress concrete bridge construction: Untopped girders and Topped girders. The design philosophy to minimize the long-term deflections for both types of cases are discussed. Appendix A outlines the basic design information that is common for both cases of construction.

A.2 DESIGN PARAMETERS

The prototype bridge designs were developed based on the design parameters and assumptions summarized in Table A.1. These cross-sectional parameters and the material properties of concrete and steel were chosen based on the typical values generally adopted by TxDOT in accordance with the AASHTO LRFD Specifications (AASHTO 2017). The pretensioning steel of the girder segments consists of 0.6 in. diameter Grade 270 low

relaxation strands having an ultimate tensile strength $f_{pu} = 270\ ksi$. The initial stress in the pretensioning strands at transfer $f_{pi} = 0.70 f_{pu} = 189\ ksi$. The following were the common parameters selected for the design examples:

- Approach span of the bridge is 100 ft
- Bridge is designed for 3 lanes
- T551 type railing on each side
- AASHTO HL-93 loading

Table A-1: Bridge Design Parameters (Hueste et al., 2012)

Parameter		**Value**
Total bridge width		46 ft
Unit weight of concrete (Precast), w_c		150 lb/ft^3
Unit weight of asphalt wearing surface, w_s		140 lb/ft^3
Precast Concrete Strength at release, f'_{ci}		6 ksi
Precast Concrete Strength at service, f'_c		8 ksi
Modulus of elasticity, E_c		5255 ksi
Coefficient of Thermal Expansion of Concrete		$6 \times 10^{-5}/F$
Relative Humidity		65%
Mild Steel	Yield Strength, f_y	60 ksi
	Modulus of Elasticity, E_s	29,000 ksi
Prestressing Steel	Strand diameter	0.6 in.
	Ultimate tensile strength, f_{pu}	270 ksi
	Yield Strength, f_{py}	$0.9 f_{pu}$
	Modulus of Elasticity, E_p	28,500 ksi
	Force per strand	32.8 kips
Pretensioning	Stress limit at transfer, f_{pi}	$f_{pi} \leq 0.75 f_{pu}$
	Stress limit at service, f_{pe}	$f_{pe} \leq 0.8 f_{py}$

The primary designs presented in this section were developed according to the state-of-the-art and practice of girder bridges. Following were the basic assumptions which were used for these primary designs (Hueste el al., 2012).

- The construction was assumed to be done using temporary intermediate diaphragms of structural steel shapes. The negligible weight of these temporary components was not considered in the calculations.
- An 8 in. thick asphalt wearing surface was used but was not considered part of the structural section and was treated as additional superimposed dead load.
- The sign convention used for preliminary designs considered tension as positive and compression as negative.
- Negative deflection value indicated upward camber while a positive deflection means sagging.

A.3 DEAD LOADS

Dead loads considered in the design were girder and slab self-weight, asphalt surface weight and the weight of guard rails. Typical TxDOT railing T551 was considered for the design. The girder weight and deck weight acts on the non-composite sections whereas the railing load and the wearing surface load acts on the composite actions during service. The load due to deck, asphalt surface and guard rails was distributed to the individual girder based on center-to-center spacing between the girders.

A.4 LIVE LOADS

HL-93 loading was considered which is as per AASHTO LRFD Specification (AASHTO 2017) Article 3.6.1.2. The vehicular live load should consist of (a) Design Truck or Design Tandem load and (b) Lane load. The live load moments and shear forces including the dynamic load effect were distributed to the individual girders using distribution factors (DFs) as specified in AASHTO LRFD Bridge Design Specifications (AASHTO 2017) Article 4.6.2.2.2.

A.4.1 Design Truck Load

According to HL-93, the design truck loads are taken as axle loads of 8-kip, 32-kip and 32-kip for front axle, and two rear axles respectively. These loads are spaced 14 ft apart and increased by 33% to account for the impact factor (AASHTO 2017, Table 3.6.2.1-1). The point loads were rearranged in such a fashion that the load is symmetrically distributed on the both the supports like (20-kip + 32-kip + 20-kip). The 32-kip load is acting at the center of the span while the 20-kip load are spaced at 14 ft from center on either side.

A.4.2 Design Tandem Load

The design tandem consists of a pair of 25-kip axles spaced 4 ft apart. A factor of 1.33 was multiplied to the axle loads to account for dynamic load effects (AASHTO 2017, Table 3.6.2.1-1).

A.4.3 Design Lane Load

The design lane load was taken as 0.64 kip/ft uniformly distributed along the longitudinal span and were not subjected to dynamic impact factor.

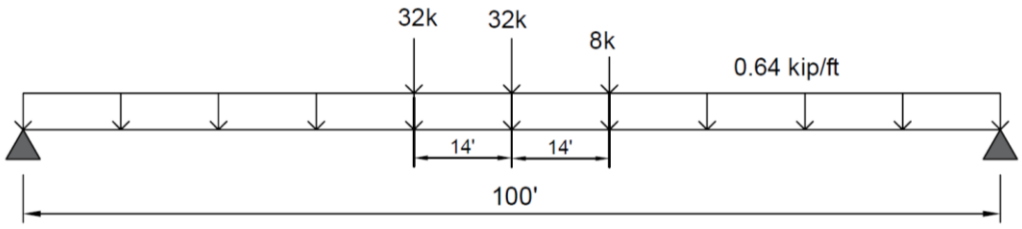

Figure A-1. Design Truck and Design Lane Load

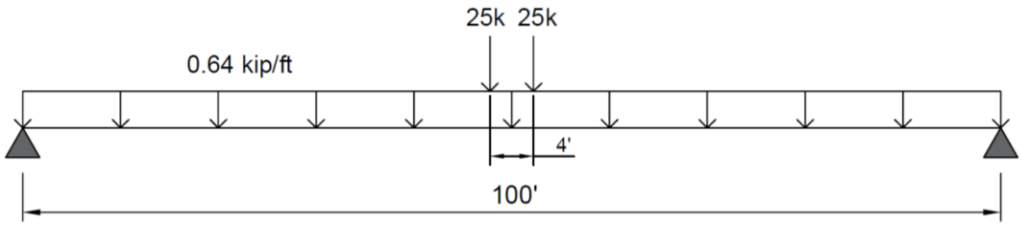

Figure A-2. Design Tandem and Design Lane Load

Table A-2: Distribution factors for Live Load (AASHTO 2017, Table 4.6.2.2.2 and 4.6.2.2.3)

Live Load Distribution Factors	Distribution Factors	Range of Applicability
For Moment in Interior Beams	One Design Lane Loaded: $0.06 + \left(\frac{S}{14}\right)^{0.4} \left(\frac{S}{L}\right)^{0.3} \left(\frac{K_g}{12Lt_s^3}\right)^{0.1}$ Two or more Design Lanes Loaded: $0.075 + \left(\frac{S}{9.5}\right)^{0.6} \left(\frac{S}{L}\right)^{0.2} \left(\frac{K_g}{12Lt_s^3}\right)^{0.1}$	$3.5 \leq S \leq 16$ $4.5 \leq t_s \leq 12$ $20 \leq L \leq 240$ $N_b \geq 4$ $10{,}000 \leq K_g \leq 7{,}000{,}000$
For Moment in Exterior Beam	One Design Lane Loaded: Lever Rule Two or more Design Lanes Loaded: $g = eg_{interior}$ $e = 0.77 + \frac{d_e}{9.1}$	$-1.0 \leq d_e \leq 5.5$
For Shear in Interior Beams	One Design Lane Loaded: $0.36 + \left(\frac{S}{25}\right)$ Two or more Design Lanes Loaded: $0.2 + \left(\frac{S}{12}\right) - \left(\frac{S}{35}\right)^2$	$3.5 \leq S \leq 16$ $4.5 \leq t_s \leq 12$ $20 \leq L \leq 240$ $N_b \geq 4$
For Shear in Exterior Beam	One Design Lane Loaded: Lever Rule Two or more Design Lanes Loaded: $g = eg_{interior}$ $e = 0.6 + \frac{d_e}{10}$	$-1.0 \leq d_e \leq 5.5$

where, S = center to center spacing between girders (ft); L = span of the beam (ft); K_g = stiffness of the non-composite section (in^4); t_s = thickness of deck concrete ($in.$); N_b = number of girders in the cross-section; d_e = overhang width of the roadway (ft); and $g_{interior}$ = spacing between the exterior and first interior girder (ft).

A.5 ALLOWABLE STRESS LIMITS

The stresses at various stages of construction were checked to ensure that the stress in concrete is less than the limit specified by AASHTO 2017 Article 5.9.2.3. The stress limits were based on the compressive strength for the precast concrete of 8.5 ksi at service and 6 ksi at release. The concrete strength for the deck concrete at service was 4 ksi. The reduction factor, $\phi_w = 1.0$ when the web and flange slenderness ratio calculated according to AASHTO 2017 Article 5.6.4.7.1 is less than or equal to 15. The stress limits for girder are summarized in Table A-3 and the stress limits for deck are summarized in Table A-4.

Table A-3: Allowable Stress Limits for precast Girder

Loading Stage	**Type of Stress**	**Allowable Stress Limits (ksi)**
Initial stage at transfer	Compressive	$-0.6f'_{ci} = -3.60$
	Tensile	$0.24\sqrt{f'_{ci}} = 0.59$
Intermediate stage at service (effective prestress and permanent loads)	Compressive	$-0.45f'_c = -3.83$
	Tensile	$0.19\sqrt{f'_c} = 0.55$
Final stage at service (effective prestress, permanent loads as well as transient loads)	Compressive	$-0.60\phi_w f'_c = -5.10$
	Tensile	$0.19\sqrt{f'_c} = 0.55$

Table A-4: Allowable Stress Limits for deck concrete

Loading Stage	**Type of Stress**	**Allowable Stress Limits (ksi)**
Final stage at service (effective prestress, permanent loads as well as transient loads)	Compressive	$-0.60\phi_w f'_c = -2.40$
	Tensile	$0.19\sqrt{f'_c} = 0.38$

A.6 LIMIT STATES

A.6.1 Service Limit State

For prestressed concrete members, the service load design typically governs, therefore the prestressed concrete members are designed for service stresses and then checked for strength. The design satisfying service load criteria generally satisfies the strength limit state. Service load stresses were checked during various stages of construction for each design. The service limit state was based on AASHTO 2017 Article 3.4.1.

Service I – Compression in prestressed concrete components was checked using this load combination.

$$Q = 1.00(DC) + 1.00(DW) + 1.00(LL + IM) \quad \text{(A-1)}$$

Service III – Tensile stresses in prestressed concrete components were checked using this load combination.

$$Q = 1.00(DC) + 1.00(DW) + 1.00(LL + IM) \quad \text{(A-2)}$$

where, $\gamma_{LL} = 0.8$ for multiple presence factor (From AASHTO 2017 Table 3.4.1-4)

A.6.2 Flexural limit state

The flexural limit state was based on the provisions from AASHTO LRFD Bridge Design Specifications (AASHTO 2017) Article 5.6.3 based on Strength I limit state. The load factors were taken from AASHTO LRFD Bridge Design Specifications (AASHTO 2017) Table 3.4.1-1. The flexural strength limit state needs to be checked to ensure safety at the ultimate load conditions. The flexural strength limit state design requires the reduced nominal moment capacity of the member to be greater than the factored ultimate design moment, expressed as follows:

$$\phi M_n \geq M_u \tag{A-3}$$

$$M_u = 1.25(M_{DC}) + 1.5(M_{DW}) + 1.75(M_{LL+IM}) \tag{A-4}$$

where M_u = ultimate flexural demand; M_{DC} = moment due to dead loads except wearing surface; M_{DW} = moment due to wearing surface load; M_{LL+IM} = moment due to live load and impact; M_n = flexural resistance of the section; and ϕ = strength reduction factor = 1.0 for tension-controlled sections and = 0.75 for compression-controlled sections (AASHTO 2017, Article 5.5.4.2).

The strength reduction factor for sections in transitions was calculated using:

$$0.75 \leq \phi = 0.75 + \frac{0.25(\varepsilon_t - 0.002)}{(0.003)} \leq 1.0 \qquad \text{(AASHTO Eq. 5.5.4.2-1)}$$

A.6.3 Shear limit state

The shear limit state check was based on the provisions from AASHTO LRFD Bridge Design Specifications (AASHTO 2017) Article 5.7.3.3 and is based on Strength I limit state. The load factors were taken from AASHTO LRFD Bridge Design Specifications (AASHTO 2017) Table 3.4.1-1. The Modified Compression Field Theory (MCFT) approach was adopted for transverse shear reinforcement. For MCFT, the nominal shear resistance (V_n) is assumed to be sum of three forces: force in stirrups (V_s), vertical component of force in concrete (V_c) and; vertical component of any harped or draped prestressing strand (V_p). MCFT accounts for the combined effect of axial load, flexure and prestressing when designing for shear. The shear strength of concrete is based on the angle of strut. The ultimate shear demand is determined by:

$$V_u = 1.25(V_{DC}) + 1.5(V_{DW}) + 1.75(V_{LL+IM}) \quad \text{(A-5)}$$

$$\phi V_n \geq V_u \quad \text{(A-6)}$$

where V_{DC} = shear force due to dead loads except wearing surface; V_{DW} = shear force due to wearing surface load; V_{LL+IM} = shear force due to live load and impact; V_n = shear resistance of the section; and ϕ = strength reduction factor = 0.9 for normal-weight prestressed concrete members (AASHTO 2017, Article 5.5.4.2).

Overall, the shear resistance is taken as the smaller of:

a. $V_n = V_p + V_c + V_s$ (AASHTO Eq. 5.7.3.3-1)

b. $V_n = 0.25 f_c' b_v d_v + V_p$ (AASHTO Eq. 5.7.3.3-2)

in which,

$$V_c = 0.0316 \beta \lambda \sqrt{f_c'} b_v d_v \quad \text{(AASHTO Eq. 5.7.3.3-3)}$$

$$V_S = \frac{A_v f_y d_v (\cot\theta + \cot\alpha) \sin\alpha}{s} \quad \text{(AASHTO Eq. 5.7.3.3-4)}$$

where, θ = angle of strut with the horizontal axis of member; b_v = minimum web width within the member depth; d_v = effective shear depth taken as greater of $0.9d_e or\ 0.72h$; s = spacing of transverse reinforcement; β = factor indicating ability of diagonally cracked concrete to transmit tension and shear; A_v = area of transverse reinforcement within distance s; V_p = component of prestressing force in the direction of the shear force; λ = concrete density modification factor; and α = angle of inclination of transverse reinforcement to longitudinal axis.

A.7 DEFLECTION

The deflection limit state is checked to ensure that there are not excessive vibrations in the bridge and also to limit the cracking in members. The deflection due to axle point loads may be calculated using conjugate beam method. Deflection due to the uniformly distributed lane load was calculated using $\frac{5WL^3}{384EI}$ and added to deflection due to the axle point loads to obtain the maximum deflection for the approach span of bridge. The total stiffness of the composite section was based on the transformed moment of inertia of the deck. According to AASHTO LRFD Bridge Design Specification (AASHTO 2017) Article 3.6.1.3.2, the deflection should be taken as the larger of:

a. Design truck alone
b. 25 percent of design truck load and full design lane load

This deflection was checked with the maximum allowable deflection as per AASHTO LRFD Specification (AASHTO 2017) Article 2.5.2.6.2 which is $L/800$; where L is in ft.

A.8 CREEP AND SHRINKAGE

Long-term camber and deflections are significantly affected by creep and shrinkage of concrete. When loaded, the concrete deforms elastically initially and will continue to deform with the passage of time. Even if the load is removed, the total deformation is only partially recoverable. This continued deformation is called creep. The creep deflection is calculated by multiplying the creep coefficients by the corresponding elastic deflections.

During the drying process, volume of the concrete decreases and causes the beam to decrease in length. This contributes to prestress losses, which in turn results in decreased

beam camber with time. Thus, the prediction of shrinkage strain to be experienced by the girder is significant.

A.8.1 ACI 209R-92

A.8.1.1 Creep

The predicted creep coefficient $\phi(t, t_0)$ is the ratio of a creep strain to initial strain.

$$\phi(t, t_0) = \frac{(t - t_0)^{\psi}}{d + (t - t_0)^{\psi}} \phi_u \tag{A-7}$$

For the standard conditions, the average value for the ultimate creep coefficient ϕ_u is:

$$\phi_u = 2.35 \tag{A-8}$$

For conditions other than the standard conditions, the value of the ultimate creep coefficient ϕ_u needs to be modified by correction factors:

$$\phi_u = 2.35\gamma_C \tag{A-9}$$

in which, $\gamma_C =$ the cumulative product of the applicable correction factors for creep defined as:

$$\gamma_C = \gamma_{C,to} \cdot \gamma_{C,RH} \cdot \gamma_{C,vs} \cdot \gamma_{C,s} \cdot \gamma_{C,\psi} \cdot \gamma_{c,\alpha} \tag{A-10}$$

where, $\frac{V}{S} =$ Volume-surface ratio in inches; $d =$ Days (constant); $\psi =$ Constant for a given member shape and size that defines the time-ratio part; $(t - t_0) =$ the time since application of load; $\alpha =$ the air content in percent; and $(t - t_c) =$ the time from the end of the initial curing.

Table A-5: Correction factors for Creep (ACI 209R-92)

Correction factors	Creep
Curing	$\gamma_{c,to} = 1.25t_0^{-0.118}$ for moist curing $\gamma_{c,to} = 1.13t_0^{-0.094}$ for steam curing
Ambient relative humidity	$\gamma_{C,RH} = 1.27 - 0.67h,\ h \geq 0.40$ $\gamma_{C,RH} \geq 1$ for $h < 0.40$
Size of member	Members with V/S ≠ 1.5in., or average thickness ≠ 6in.: $\gamma_{c,vs} = \frac{2}{3}\left(1 + 1.13e^{\{-0.54(V/S)\}}\right)$ For average thickness of a member < 6in. or V/S < 1.5in., factors are given in ACI 209R-92. For the average thickness of members > 6in. and up to 15in.: $\gamma_{c,d} = 1.14 - 0.092(V\ /\ S)$ for $(t - t_0) \leq 1\ year$ $\gamma_{c,d} = 1.10 - 0.068(V/S)$ for $(t - t_0) > 1\ year$
Slump	$\gamma_{C,s} = 0.82 + 0.067s$
Fine aggregate content	$\gamma_{C,\psi} = 0.88 + 0.0024\ \psi$
Air content	$\gamma_{c,\alpha} = 0.46 + 0.09\ \alpha \geq 1$

A.8.1.2 Shrinkage

The shrinkage strain $\varepsilon_{sh}(t, t_0)$ at age of concrete t (days), measured from the start of drying at t_c (days), is calculated by:

$$\varepsilon_{sh}(t, t_c) = \frac{(t - t_c)^{\alpha}}{f + (t - t_c)^{\alpha}} \varepsilon_{shu} \tag{A-11}$$

For the standard conditions, at ambient relative humidity of 40%, the average value suggested for the ultimate shrinkage strain ε_{shu}, is:

$$\varepsilon_{shu} = 780 \times 10^{-6} \tag{A-12}$$

For conditions other than the standard conditions, ε_{shu} needs to be modified for correction factors depending on particular conditions:

$$\varepsilon_{shu} = 780\gamma_{sh} \times 10^{-6} \tag{A-13}$$

in which, γ_{SH} = the cumulative product of the applicable correction factors for shrinkage

$$\gamma_{sh} = \gamma_{sh,tc} \cdot \gamma_{sh,RH} \cdot \gamma_{sh,vs} \cdot \gamma_{sh,s} \cdot \gamma_{sh,\psi} \cdot \gamma_{sh,c} \cdot \gamma_{sh,\alpha} \tag{A-14}$$

For any method, γ_{sh} should not be taken less than 0.2. Also, $\gamma_{sh}\varepsilon_{shu} \geq 100 \times 10^{-6}$ should be used if concrete is under seasonal wetting and drying cycles and $\gamma_{sh}\varepsilon_{shu} \geq 150 \times 10^{-6}$ if concrete is under sustained drying conditions.

Table A-6: Correction factors for Shrinkage (ACI 209R-92)

Correction factors	**Shrinkage**
Curing	$\gamma_{sh,tc} = 1.202 - 0.2337\log(t_c)$
Ambient relative humidity	$\gamma_{sh,RH} = 1.4 - 1.02h, \quad 0.4 \leq h \leq 0.8$ $\gamma_{sh,RH} = 3 - 3h, \quad 0.8 \leq h \leq 1$
Size of member	Members with V/S ≠ 1.5in., or average thickness ≠ 6in.: $\gamma_{sh,vs} = 1.2e^{\{-0.12(V/S)\}}$ For average thickness of a member < 6in. or V/S < 1.5in., factors are given in ACI 209R-92. For the average thickness of members > 6in. and up to 15in.: $\gamma_{sh,d} = 1.23 - 0.152(V/S)$ for $(t - t_0) \leq 1\ year$ $\gamma_{c,d} = 1.23 - 0.116(V\ /\ S)$ for $(t - t_0) > 1\ year$
Slump	$\gamma_{C,s} = 0.89 + 0.041s$
Fine aggregate content	$\gamma_{sh,\psi} = 0.90 + 0.002\,\psi$
Air content	$\gamma_{sh,c} = 0.75 + 0.00036c$

A.8.2 *fib* 2010

A.8.2.1 Creep

The creep coefficient $\varphi(t, t_0)$ may be calculated from:

$$\varphi(t, t_0) = \varphi_{bc}(t, t_0) + \varphi_{dc}(t, t_0) \qquad (\textit{fib}\ 2010\ \text{Eq. 5.1-63})$$

where, $\varphi_{bc}(t, t_0) =$ basic creep coefficient and $\varphi_{dc}(t, t_0) =$ drying creep coefficient

A.8.2.2 Shrinkage

The total shrinkage strain or swelling strain strains $\varepsilon_{cs}(t, t_s)$ may be calculated as:

$$\varepsilon_{cs}(t, t_s) = \varepsilon_{cbs}(t) + \varepsilon_{c\,ds}(t, t_s) \qquad (\textit{fib}\ 2010\ \text{Eq. 5.1-75})$$

where, shrinkage is subdivided into the basic shrinkage $\varepsilon_{cbs}(t)$ which occurs even if no moisture loss is possible and the drying shrinkage $\varepsilon_{c\,\mathrm{ds}}(t, t_s)$ giving the additional shrinkage if moisture loss occurs.

A.8.3 AASHTO LRFD (2017)

A.8.3.1 Creep

The creep coefficients can be calculated as:

$$\Psi(t, t_i) = 1.9 k_s k_{hc} k_f k_{td} t_i^{-0.118} \qquad (\text{AASHTO Eq. 5.4.2.3.2-1})$$

where, $k_s =$ factor for the effect of the volume-to-surface ratio of the component; $k_{hc} =$ humidity factor for creep; $k_f =$ factor for the effect of concrete strength; and $k_{td} =$ time development factor;

in which,

$$k_s = 1.45 - 0.13\left(\frac{V}{S}\right) \geq 1.0 \qquad (\text{AASHTO Eq. 5.4.2.3.2-2})$$

$$k_{hc} = 1.56 - 0.008H \qquad \text{(AASHTO Eq. 5.4.2.3.2-3)}$$

$$k_f = \frac{5}{1 + f'_{c_i}} \qquad \text{(AASHTO Eq. 5.4.2.3.2-4)}$$

$$k_{td} = \frac{t}{12\left(\frac{100 - 4f'_{ci}}{f'_{ci} + 20}\right) + t} \qquad \text{(AASHTO Eq. 5.4.2.3.2-5)}$$

where, $H =$ relative humidity (%) taken from AASHTO 2017 Figure 5.4.2.3.3-1; $t =$ maturity of concrete (days); and $t_i =$ age of concrete at time of load application (day).

A.8.3.2 Shrinkage

The shrinkage ε_{sh} at time t may be taken as:

$$\varepsilon_{sh} = k_s k_{hs} k_f k_{td} 0.48 \times 10^{-3} \qquad \text{(AASHTO Eq. 5.4.2.3.3-1)}$$

$$k_{hs} = (2.00 - 0.014H) \qquad \text{(AASHTO Eq. 5.4.2.3.3-2)}$$

where, $k_{hs} =$ humidity factor for shrinkage

A.9 PRESTRESS LOSSES

The reduction in the initial prestressing force during the life of a girder is called the prestress loss. The total losses are the collective result of instantaneous losses and time-dependent losses. The instantaneous loss is due to the elastic shortening of the member while the combination of creep and shrinkage losses and the relaxation of prestressing steel are included in the time dependent losses.

During the transfer of the prestress, the axial compressive force applied to the girder causes shortening and elastic bending. The bond between the prestressing steel and concrete causes the strands to shorten, reducing the tension stress and strain. It is

dependent on several variables, including the initial force, the properties of steel, and the temperature of the prestressing strands.

The prestress losses are estimated using provisions from AASHTO LRFD Bridge Design Specifications (AASHTO 2017).

A.9.1 Total loss

In pretensioned members:

$$\Delta f_{pT} = \Delta f_{pES} + \Delta f_{pLT} \qquad \text{(AASHTO Eq. 5.9.3.1-1)}$$

where, $\Delta f_{pES} =$ losses due to elastic shortening at the time of application of prestress (ksi) and $\Delta f_{pLT} =$ losses due to long-term shrinkage and creep of concrete, and relaxation of steel (ksi);

in which,

$$\Delta f_{pES} = \frac{E_p}{E_{ct}} f_{cgp} \qquad \text{(AASHTO Eq. 5.9.3.2.3a-1)}$$

where, $f_{cgp} =$ the concrete stress at the center of gravity of prestressing tendons due to the prestressing force immediately after transfer and the self-weight of the member at the section of maximum (ksi); $E_p =$ elastic modulus of prestressing steel (ksi); and $E_{ct} =$ modulus of elasticity of concrete at transfer or time of load application (ksi).

A.9.2 Approximate estimate of time-dependent losses

The long-term prestress loss, due to creep of concrete, shrinkage of concrete, and relaxation of steel shall be estimated as:

$$\Delta f_{pLT} = 10.0\frac{f_{pi}A_{ps}}{A_g}\gamma_h\gamma_{st} + 12.0\gamma_h\gamma_{st} + \Delta f_{pR} \quad \text{(AASHTO Eq. 5.9.3.3-1)}$$

$$\gamma_h = 1.7 - 0.01H \quad \text{(AASHTO Eq. 5.9.3.3-2)}$$

$$\gamma_s = \frac{5}{(1 + f'_{ci})} \quad \text{(AASHTO Eq. 5.9.3.3-3)}$$

where, f_{pi} = prestressing steel stress immediately prior to transfer (ksi); γ_h = correction factor for relative humidity of the ambient air; γ_{st} = correction factor for specified concrete strength at time of prestress transfer to the concrete member; and Δf_{pR} = an estimate of relaxation loss (ksi).

A.9.3 Refined estimates of time-dependent losses

The change in prestressing steel stress due to time-dependent loss, Δf_{pLT}, shall be determined as:

$$\Delta f_{pLT} = \left(\Delta f_{pSR} + \Delta f_{pCR} + \Delta f_{pR1}\right)_{id} + \left(\Delta f_{pSD} + \Delta f_{pCD} + \Delta f_{pR2} - \Delta f_{pSS}\right)_{df} \quad \text{(AASHTO Eq. 5.9.3.4.1-1)}$$

in which, $\left(\Delta f_{pSR} + \Delta f_{pCR} + \Delta f_{pR1}\right)_{id}$ = prestress loss due to creep of girder concrete between time of deck placement and final time (ksi) from Article 5.9.3.4.2 and $\left(\Delta f_{pSD} + \Delta f_{pCD} + \Delta f_{pR2} - \Delta f_{pSS}\right)_{df}$ = sum of time-dependent prestress losses after deck placement (ksi) from Article 5.9.3.4.3; where, Δf_{pSR} = prestress loss due to shrinkage of girder concrete between transfer and deck placement (ksi); Δf_{pCR} = prestress loss due to creep of girder concrete between transfer and deck placement (ksi); Δf_{pR1} = prestress loss due to relaxation of prestressing strands between time of transfer and deck placement (ksi); Δf_{pR2} = prestress loss due to relaxation of prestressing strands in composite section

between time of deck placement and final time (ksi); Δf_{pSD} = prestress loss due to shrinkage of girder concrete between time of deck placement and final time (ksi); Δf_{pCD} = prestress loss due to creep of girder concrete between time of deck placement and final time (ksi); and Δf_{pSS} = prestress gain due to shrinkage of deck in composite section (ksi).

A.10 LONG-TERM MULTIPLIERS

Using Martin's (1977) multipliers, the camber and deflection may be found only for the most probable case of girder age at erection which is 6 to 8 weeks. The multipliers do not take into consideration if the girders are erected at an early age or mature age. Also, these multipliers do not reflect the characteristics of the modern bridge girders. Therefore, the multipliers for topped case at-erection and long-term service are rederived for early age girders and mature age girders using the actual ratio of non-composite moment of inertia to the composite moment of inertia of the section based on the procedure given by Martin (1977).

A.10.1 Erection Camber

Martin (1977) assumes that most of the girders are erected between 40 to 60 days following casting and that the long-term factors will have reached about 40 to 60 percent of ultimate in that time. Then the multiplier for the erection is:

For most probable case, $$\mu_{de} = 0.5\mu_{df}$$ (Martin Eq. 6)

For early age case, $$\mu_{de} = 0$$ (A-15)

For mature age case, $$\mu_{de} = \mu_{df}$$ (A-16)

where, μ_{df} = long-time factor which is applied to the initial deflection caused by the dead weight of the member;

in which,

$$\mu_{df} = \frac{E_{c_i}}{E_c}\mu_b = 1.7 \qquad \text{(Martin Eq. 5)}$$

where, μ_b = base factor for additional long-time deflection ($\mu_b = 2$) and; E_{c_i} = release strength of precast prestressed members ($E_{c_i} = 0.85E_c$).

Therefore, the multiplier applied to the initial member weight deflection is:

For most probable case, $1 + \mu_{de} = 1.85$ (Martin Eq. 7)

For early age case, $1 + \mu_{de} = 1.00$ (A-17)

For mature age case, $1 + \mu_{de} = 2.70$ (A-18)

A.10.2 Long-time Camber

In case of composite girders, the final multipliers are modified to include the effect of the increased moment of inertia after the topping is added. The difference between the non-composite factors at erection and final should be multiplied by the ratio of non-composite to composite moment of inertia, $I_0 \,/\, I_c$. In the particular design example considered, the ratio $I_0/I_c = 0.45$. The long-time factor then becomes:

$$\mu_{dfc} = \mu_{de} + \left(\mu_{df} - \mu_{de}\right)(I_0 \,/\, I_c) \qquad \text{(Martin Eq. 12)}$$

The long-time multiplier applied to the initial deflection is:

For most probable case, $1 + \mu_{dfc} = 2.23$ (A-19)

For early age case, $1 + \mu_{dfc} = 1.76$ (A-20)

For mature age case, $$1 + \mu_{dfc} = 2.70 \qquad \text{(A-21)}$$

The immediate deflection caused by the placement of the deck concrete is calculated using the non-composite section properties. Therefore, the long-time factor for the composite topping is also modified to include the effect of higher moment of inertia of the composite section.

$$\mu_t = \mu_b (I_0 \,/\, I_c) = 0.89 \qquad \text{(Martin Eq. 16)}$$

$$1 + \mu_t = 1.89 \qquad \text{(Martin Eq. 17)}$$

APPENDIX B

DESIGN EXAMPLE

B.1 OVERVIEW

This chapter presents the procedure and values used for design examples. The design example includes prestress design, stress checks, ultimate flexural strength checks, deflection checks, and shear design. The AASHTO LRFD Bridge Design Specifications (AASHTO 2017) are referenced in the design examples.

B.2 CROSS-SECTIONAL PROPERTIES

The bridge has a total width of 46 ft and a total roadway width of 44 ft. A wearing surface of thickness 2 in. is considered in the design. TxDOT standard T551 type rails of 1 ft width on each side is considered for the design.

The cross section for the untopped case includes 5 numbers of Tx62 girder spaced at 9.5 ft center-to-center, with a monolithic cast flange of width 8 ft and thickness 8 in. The overhang on each side is 4 ft.

The cross section for the topped case includes 5 numbers of Tx62 girder spaced at 10 ft center-to-center, acting compositely with a cast-in-place flange of width 10 ft and thickness 8.5 in. as per standard TxDOT specification. The overhang on each side is 3 ft.

The cross-section properties of the non-composite and composite sections are summarized in Table B-1.

Table B-1: Section properties for Untopped and Topped case

Section Property	Standard Tx62	Tx62 + 8 in. precast flange	Tx62 + 8.5 in CIP deck
Total height (in.)	62	70	70.5
Depth of N.A. from top of girder, y_t (in.)	33.7	24.5	25.7
Depth of N.A. from girder soffit, y_b (in.)	28.3	45.5	44.8
Area, A (in^2)	910	1,678	1,610
Moment of Inertia, I_x (in^4)	463,072	1,059,758	1,038,341
Section Modulus, S_{xt} (in^3)	13,733	51,807	40,379
Section Modulus, S_{xb} (in^3)	16,374	23,269	23,185

Table B-2 represents the dead weight acting on each individual girder due to various components for the untopped and topped case.

Table B-2: Dead loads for Untopped case

Component	Untopped Case		Topped case	
	Value (kip/ft)	Applied to	Value (kip/ft)	Applied to
Self-weight of girders	1.75	Girder section	0.95	Girder section
Deck weight	-	-	1.06	Girder section
Asphalt surface weight	0.22	Girder section	0.23	Composite section
Barrier weight	0.16	Girder section	0.17	Composite section

B.3 STRESS ANALYSIS

The stress analysis is carried out for all four stages of construction and service. Sample calculations for topped girder case having eccentric tendon profile is shown below.

Sample Calculations for Stress Analysis of Topped Eccentric Case

Initial Force	$F_i := 1476.47\ kip$
Eccentricity (non-composite)	$e_1 := 18\ in$
Eccentricity (composite)	$e_2 := 18\ in + 16.5\ in = 34.5\ in$
Area of girder	$A_g := 910\ in^2$
Section modulus (top)	$S_{xt} := 13732.9\ in^3$
Section modulus (bottom)	$S_{xb} := 16374.5\ in^3$
Area of composite section	$A_c := 1609.7\ in^2$
Section modulus (top)	$S'_{xtc} := 60315.7\ in^3$
Section modulus (bottom)	$S_{xbc} := 23185.1\ in^3$
Girder Moment	$M_g := 1184.9\ kip \cdot ft$
Deck Moment	$M_d := 1328.1\ kip \cdot ft$
Imposed Dead Load Moment	$M_{sidl} := 498.5\ kip \cdot ft$
Live+Impact Load Moment	$M_{LL} := 2351.3\ kip \cdot ft$

Stage - 1 At the time of release of prestress

$$\sigma_{t1} := \frac{-0.95 \cdot F_i}{A_g} + \frac{0.95 \cdot F_i \cdot e_1}{S_{xt}} - \frac{M_g}{S_{xt}} = -0.738\ ksi$$

$$\sigma_{b1} := \frac{-0.95 \cdot F_i}{A_g} - \frac{0.95 \cdot F_i \cdot e_1}{S_{xb}} + \frac{M_g}{S_{xb}} = -2.215\ ksi$$

Stage - 2 At the time of erection (after 40-60 days of girder casting)

$$\sigma_{t2} := \sigma_{t1} + \frac{0.075 \cdot F_i}{A_g} - \frac{0.075 \cdot F_i \cdot e_1}{S_{xt}} = -0.762\ ksi$$

$$\sigma_{b2} := \sigma_{b1} + \frac{0.075 \cdot F_i}{A_g} + \frac{0.075 \cdot F_i \cdot e_1}{S_{xb}} = -1.971\ ksi$$

Stage - 3 At the time of deck casting (after 40-60 days of girder casting)

$$\sigma_{t3} := \sigma_{t2} - \frac{M_d}{S_{xt}} = -1.922\ ksi$$

$$\sigma_{b3} := \sigma_{b2} + \frac{M_d}{S_{xb}} = -0.998\ ksi$$

Stage - 4 At the time of service

$$\sigma_{t4} := \sigma_{t3} + \frac{0.075 \cdot F_i}{A_c} - \frac{0.075 \cdot F_i \cdot e_2}{S'_{xtc}} - \frac{M_{sidl}}{S'_{xtc}} - \frac{M_{LL}}{S'_{xtc}} = -2.484\ ksi$$

$$\sigma_{b4} := \sigma_{b3} + \frac{0.075 \cdot F_i}{A_c} + \frac{0.075 \cdot F_i \cdot e_2}{S_{xbc}} + \frac{M_{sidl}}{S_{xbc}} + \frac{0.8 \cdot M_{LL}}{S_{xbc}} = 0.467\ ksi$$

B.4 DEFLECTION PROFILE

The deflection under dead load is calculated at different locations of the span for all four stages of construction and service. Sample calculations for topped girder case having eccentric tendon profile is shown below.

Sample Calculations for Deflection at midspan under dead loads of Topped Eccentric Case

Weight of girder	$w_g := 0.95\ \frac{kip}{ft}$
Weight of deck	$w_d := 1.06\ \frac{kip}{ft}$
Weight of imposed dead load	$w_{sidl} := 0.166\ \frac{kip}{ft}$
Length of the Span	$L := 100\ ft$
Modulus of Elasticity	$E_c := 5255.14\ ksi$
Initial Modulus of Elasticity	$E_{ci} := 0.85 \cdot E_c = \left(4.467 \cdot 10^3\right)\ ksi$
Moment of Inertia of girder	$I_g := 463072\ in^4$
Moment of Inertia of composite section	$I_c := 1038341.2\ in^4$
Immediate deflection due to girder self-weight	$\Delta_{gi} := \frac{5}{384} \cdot \frac{w_g \cdot L^4}{E_{ci} \cdot I_g} = 1.033\ in$
Immediate deflection due to prestress	$\Delta_{pi} := -\frac{F_i \cdot e_1 \cdot L^2}{8 \cdot E_{ci} \cdot I_g} = -2.313\ in$

Stage - 1 At the time of release of prestress

$$\Delta_1 := 0.95 \cdot \Delta_{pi} + \Delta_{gi} = -1.164\ in$$

Stage - 2 At the time of erection (after 40-60 days of girder casting)

$$\Delta_2 := 0.875 \cdot \Delta_{pi} \cdot 1.85 + \Delta_{gi} \cdot 1.85 = -1.832\ in$$

Stage - 3 At the time of deck casting (after 40-60 days of girder casting)

$$\Delta_d := \frac{5}{384} \cdot \frac{w_d \cdot L^4}{E_c \cdot I_g} = 0.98\ in$$

$$\Delta_3 := 0.875 \cdot \Delta_{pi} \cdot 1.85 + \Delta_{gi} \cdot 1.85 + \Delta_d \cdot 1.0 = -0.852\ in$$

Stage - 4 At the time of service

$$\Delta_{pt} := \frac{1}{8} \cdot \frac{F_i \cdot e_2 \cdot L^2}{E_c \cdot I_c} = 1.68\ in$$

$$\Delta_{sidl} := \frac{5}{384} \cdot \frac{w_{sidl} \cdot L^4}{E_c \cdot I_c} = 0.068\ in$$

$$\Delta_4 := 0.875 \cdot \Delta_{pi} \cdot 2.23 + \Delta_{gi} \cdot 2.23 + \Delta_d \cdot 1.89 + 0.075 \cdot \Delta_{pt} \cdot 1.89 + \Delta_{sidl} \cdot 3.0 = 0.088\ in$$